# ON THE PLANAR TRANSLATION OF TWO BODIES IN A UNIFORM FLOW

by

Zhi Guo and Allen T. Chwang

Sponsored by

Ocean Engineering Division
Office of Naval Research
Under Grant N00014-89-J-1581

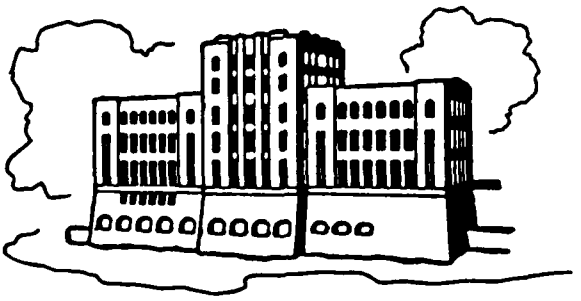



IIHR Report No. 337

Iowa Institute of Hydraulic Research
The University of Iowa
Iowa City, Iowa 52242

March 1990

# ON THE PLANAR TRANSLATION OF TWO BODIES IN A UNIFORM FLOW

by

Zhi Guo and Allen T. Chwang

Sponsored by

Ocean Engineering Division
Office of Naval Research
Under Grant N00014-89-J-1581

IIHR Report No. 337

Iowa Institute of Hydraulic Research
The University of Iowa
Iowa City, Iowa 52242

March 1990

Unclassified

SECURITY CLASSIFICATION OF THIS PAGE (When Data Entered)

| REPORT DOCUMENTATION PAGE | | READ INSTRUCTIONS BEFORE COMPLETING FORM |
|---|---|---|
| 1. REPORT NUMBER 337 | 2. GOVT ACCESSION NO. | 3. RECIPIENT'S CATALOG NUMBER |
| 4. TITLE (and Subtitle) On the Planar Translation of Two Bodies in a Uniform Flow | | 5. TYPE OF REPORT & PERIOD COVERED Technical Report |
| | | 6. PERFORMING ORG. REPORT NUMBER 337 |
| 7. AUTHOR(s) Zhi Guo and Allen T. Chwang | | 8. CONTRACT OR GRANT NUMBER(s) N00014-89-J-1581 |
| 9. PERFORMING ORGANIZATION NAME AND ADDRESS Iowa Institute of Hydraulic Research The University of Iowa Iowa City, Iowa 52242-1585 | | 10. PROGRAM ELEMENT, PROJECT, TASK AREA & WORK UNIT NUMBERS |
| 11. CONTROLLING OFFICE NAME AND ADDRESS The Ocean Engineering Division, The Office of Naval Research, 800 N Quincy Street, Arlington, Virginia 22217-5000 | | 12. REPORT DATE March 1990 |
| | | 13. NUMBER OF PAGES 52 |
| 14. MONITORING AGENCY NAME & ADDRESS(if different from Controlling Office) Office of Naval Research Resident Representative, University of Washington, 315 University District Building, 1107 N. E. 45th Street, Seattle, Washington 98105-4631 | | 15. SECURITY CLASS. (of this report) Unclassified |
| | | 15a. DECLASSIFICATION/DOWNGRADING SCHEDULE |
| 16. DISTRIBUTION STATEMENT (of this Report) Approved for Public Release; Distribution Unlimited | | |
| 17. DISTRIBUTION STATEMENT (of the abstract entered in Block 20, if different from Report) Unlimited | | |
| 18. SUPPLEMENTARY NOTES | | |
| 19. KEY WORDS (Continue on reverse side if necessary and identify by block number) Hydrodynamic Interaction Oblique Impact Translation of Three-Dimensional Bodies Potential-Flow Theory Particle Trajectories | | |

20. ABSTRACT (Continue on reverse side if necessary and identify by block number)

The general planar translation of two bodies of revolution through an inviscid and incompressible fluid is considered. The moving trajectories and the hydrodynamic interactions are computed based on the generalized Lagrange's equations of motion, including the effects of solid constraints, external forces in the plane of motion, and a uniform stream in any direction parallel to the plane of motion. In a relative coordinate system moving with the stream, the kinetic energy of the fluid is expressed as a function of six added

DD FORM 1 JAN 73 1473 EDITION OF 1 NOV 65 IS OBSOLETE S/N 0102-LF-014-6601

Unclassified

SECURITY CLASSIFICATION OF THIS PAGE (When Data Entered)

masses due to motions parallel and perpendicular to the line joining the centers of the solid pair. The exact solution of added masses in closed forms are obtained for the motion of two spheres. A new iterative formula based on the analysis of velocity potentials around each body is developed for added masses and their derivatives with respect to the separation distance due to the transversal motion. The method of successive images and the Taylor's added-mass formula are applied to determine the added masses and their derivatives due to the centroidal motion. These results are compared with the numerical solution of added masses computed by the boundary-integral method and the generalized Taylor's added-mass formula. The integral equations, in terms of surface source distributions on both surfaces, are carefully modified for obtaining accurate numerical solutions. Numerical results are given for several practical engineering problems.

## TABLE OF CONTENTS

## ABSTRACT

The general planar translation of two bodies of revolution through an inviscid and incompressible fluid is considered. The moving trajectories and the hydrodynamic interactions are computed based on the generalized Lagrange's equations of motion, including the effects of solid constraints, external forces in the plane of motion, and a uniform stream in any direction parallel to the plane of motion. In a relative coordinate system moving with the stream, the kinetic energy of the fluid is expressed as a function of six added masses due to motions parallel and perpendicular to the line joining the centers of the solid pair. The exact solution of added masses in closed forms are obtained for the motion of two spheres. A new iterative formula based on the analysis of velocity potentials around each body is developed for added masses and their derivatives with respect to the separation distance due to the transversal motion. The method of successive images and the Taylor's added-mass formula are applied to determine the added masses and their derivatives due to the centroidal motion. These results are compared with the numerical solution of added masses computed by the boundary-integral method and the generalized Taylor's added-mass formula. The integral equations, in terms of surface source distributions on both surfaces, are carefully modified for obtaining accurate numerical solutions. Numerical results are given for several practical engineering problems.



## ACKNOWLEDGEMENTS

The authors wish to express their thanks to Professor K. E. Atkinson and Professor L. Landweber for their helpful suggestions. This work was sponsored by the Ocean Engineering Division, the Office of Naval Research, under Grant N00014-89-J-1581.

# I. INTRODUCTION

The hydrodynamic interactions among solids affect the motion of each and every solid significantly in the near field. If the Reynolds number based on the size and velocity of a typical solid is sufficiently large, the inviscid irrotational-flow theory, or the potential-flow theory, can predict the real flow with sufficient accuracy and the effects due to flow separation, boundary-layer and wake generation, and vortex formation may be neglected. The validity of this assumption has been shown by Wu and Landweber[1] by comparing the prediction with the measured results on added masses. The potential-flow theory has applications in a variety of engineering situations such as the impact of floating bodies, the motion of a blunt solid around other fixed or moving boundaries, the hydrodynamic interactions on bodies due to the oncoming flow, and so on.

Hicks[2] and Herman[3] first analyzed the kinetic energy of the fluid due to the motion of two spheres along the line joining their centers, and obtained analytic solutions of added masses in terms of doublets interior to each body. Their expressions about the strengths and positions of the doublets were alternatively reduced to a set of recurrence formulas, which were suitable for computation, as shown by Landweber in the book edited by Rouse[4]. The evaluation of added masses due to the transverse motion is more complicated. Hicks[2] used the method of successive images again and represented the added masses in terms of distributed and isolated dipoles; however, he was able to calculate only a few images owing to the complexity of the calculation. Mitra[5] and Shail[6] applied the method of successive images to the calculation of potential field surrounding both spheres, and obtained an analytic solution for the Dirichlet problem in electrostatics. They took two sets of spherical polar coordinates at the centers of each sphere and obtained a set of unknown coefficients involved in the series expansion of velocity potential by applying the Neumann-Liouville iteration process. By changing the images of point sources to dipoles, we can extend their analysis to determine the hydrodynamic interactions between two spheres moving along their centerline. The numerical solutions of the potential field due to either a moving spherical body in the inviscid flow (Neumann boundary-value problem) or a charged spherical body (Dirichlet boundary-value problem) were reported in detail by Atkinson[7],[8],[9], who also discussed the boundary-integral approach and

evaluated various solution techniques for solving the integral equations. A more general numerical model, also based on the boundary-integral method, for interaction problems of two bodies has been developed by Landweber and Chwang[10]. However, their results indicate that the numerical error becomes large when two bodies are close to each other. The motion of a solid, influenced by hydrodynamic interactions, was solved by Lamb[11], who applied the Lagrange's equations of motion in the generalized coordinates and related the fluid inertia to the equations of motion by means of the kinetic energy of the fluid. Recently, Guo and Chwang[12] applied Lamb's result to the oblique motion of two circular cylinders. They also modified the integral equations for the surface source distributions so that, when two circles were close to each other, the steep peak-values in the integrands were eliminated. In their example, very good agreement of the numerical result with the exact solution was obtained with the Gaussian quadrature formula.

In previous studies of three-dimensional solids through a fluid, much attention has been focused on the centroidal motion of two symmetric bodies, very little on the oblique motion. This is mainly due to difficulties associated with the added-mass evaluation, especially when two bodies are very close to each other. Thus, development and modifications on numerical techniques are highly desirable for accurate solutions.

The first objective of the present work is to consider the general planar translations of two bodies of revolution which are symmetric with respect to, and have their axes of rotation perpendicular to, the plane of motion. The Lagrange's equations of motion will be generalized for the trajectories of moving bodies, including the effects of solid constraints, external forces in the plane of motion, and an unbounded uniform stream in any direction parallel to the plane of motion. The second objective is to obtain the exact solution of added masses due to the transverse motion of two spheres. This solution, together with that for the centroidal motion of two spheres, will be used to examine the reliability of numerical results. The third objective is to modify the integral equations which govern the source distributions on each solid surface, and to improve the accuracy of numerical results. We shall consider the case of two spheres as an example and compare the numerical result with the exact solution.

The generalization of equations of motion for two bodies in translation is presented in Section 2. The transformation of coordinates, in which the evaluation of added masses for two bodies of revolution may become simple, is also given in this section. In Section 3, we are concerned with analytical solutions of added masses due to the centroidal and transversal motions of two spheres. We shall develop an iterative formula to calculate the unknown coefficients involved in the series expansion of velocity potentials and to determine the related added masses. The numerical solution of added masses for the two-sphere problem is given in Section 4. The set of integral equations governing the source distributions on the surfaces is modified in order to improve the ill-behaved integration when two bodies are close to each other. The reliability of numerical solutions of the integral equations obtained by the Gauss-Seidel iterative method and the Gaussian quadrature formula is examined by comparing them with the analytic solutions. Several examples are given and discussed in Section 5. Finally, conclusions are presented in Section 6.

## II. EQUATIONS OF MOTION

Consider two solids translating in an unbounded, inviscid, and incompressible fluid which moves with a uniform velocity $\mathbf{U}_0$ at infinity. Let $\mathbf{x}_\alpha$ and $\mathbf{U}_\alpha$ denote the instantaneous position and velocity vectors of body $\alpha$ ($\alpha$ = 1,2) in a relative coordinate system moving with the uniform flow; that is,

$$\mathbf{U}_\alpha = \mathbf{u}_\alpha - \mathbf{U}_0, \tag{1}$$

where $\mathbf{u}_\alpha$ is the absolute velocity of body $\alpha$.

From Lamb[11], the force acting on body $\alpha$ by the fluid, due to hydrodynamic interactions, is governed by Lagrange's equations of motion in generalized coordinates,

$$F_{i\alpha} = -\frac{d}{dt}\frac{\partial T}{\partial U_{i\alpha}} + \frac{\partial T}{\partial x_{i\alpha}}, \tag{2}$$

where t is the time, $U_{i\alpha}$ and $x_{i\alpha}$ denote the i-th (i = 1, 2, 3 in general) components of $\mathbf{U}_\alpha$ and $\mathbf{x}_\alpha$ respectively, and T is the kinetic energy of the fluid. If there is an external force $E_{i\alpha}$ acting on body $\alpha$

of mass $M_\alpha$ in addition to the force due to the fluid pressure, the equations of motion become

$$E_{i\alpha} + F_{i\alpha} = M_\alpha \frac{dU_{i\alpha}}{dt} \qquad \text{(no sum on } \alpha) \quad . \tag{3}$$

The kinetic energy T in equation (2) is given by the integration over the solid surfaces,

$$2T = -\rho \int \phi \frac{\partial \phi}{\partial n} dS \quad , \tag{4}$$

where $\phi$ is the velocity potential, n is the unit outward normal of each surface and $\rho$ is the fluid density. In the relative coordinates moving with the uniform stream at infinity, the fluid is at rest at infinity and disturbed only by motions of bodies, and the flow is therefore irrotational. The velocity potential $\phi$ satisfies the Laplace equation and may be expressed as

$$\phi = \phi_{i\alpha} U_{i\alpha}, \tag{5}$$

where $\phi_{i\alpha}$ is the velocity potential due to the unit velocity of body $\alpha$ in the i-th direction. Summation on the repeated indices is implied unless indicated otherwise. From equations (4) and (5), the kinetic energy can be expressed as (see Landweber and Chwang[10])

$$2T = A_{i\alpha j\beta} U_{i\alpha} U_{j\beta} \qquad (i, j = 1,2,3 \text{ and } \alpha, \beta = 1,2), \tag{6}$$

where

$$A_{i\alpha j\beta} = A_{j\beta i\alpha} = -\rho \int_{S_\beta} \phi_{i\alpha} \frac{\partial \phi_{j\beta}}{\partial n_\beta} dS \quad \text{(no sum on } \beta) \tag{7}$$

are added masses. Referring to the expression of hydrodynamic forces given by Landweber et al.[13], we can describe the general translations of two bodies in the relative coordinates by

$$M_\alpha \frac{dU_{i\alpha}}{dt} = E_{i\alpha} - A_{i\alpha j\beta} \frac{dU_{j\beta}}{dt} - \frac{\partial A_{i\alpha j\beta}}{\partial s_k} (U_{k1} - U_{k2}) U_{j\beta} + \frac{1}{2} U_{j\beta} U_{m\lambda} \frac{\partial A_{j\beta m\lambda}}{\partial s_i} (\delta_{\alpha 1} - \delta_{\alpha 2})$$

$$\text{(no sum on } \alpha) \quad , \tag{8}$$

where $s_k$ (k=1,2,3 in general) is the k-th component of $(x_1 - x_2)$. There are six differential equations

in (8) for two bodies translating in three dimensions. The initial conditions required for solutions of (8) are given based on physical problems.

The first integration of equation (8) yields either the velocity components of each solid relative to the uniform flow at any time instant, or the unknown forces acting on bodies due to solid constraints; and the second integration gives the trajectories of each body. Since the rotational motion is not considered in the present derivation, the equations of motion (8) is applicable to (i) the translation of two spheres in three dimensions, (ii) the planar translation of two bodies of revolution which are symmetric with respect to, and have their rotating axes perpendicular to, the plane of motion, and (iii) the centroidal translation of two bodies which are symmetric with respect to the centerline. In these three cases, the rotation of each body vanishes since the moments due to the hydrodynamic interactions are zero. However, in the present study, we will focus our attention on the first two cases.

For the planar translation of two bodies in the xy-plane (Fig. 1), we shall use the simpler notation (i, j = 1,2)

$$U_{i1} = U_i, \qquad E_{i1} = E_i, \qquad U_{i2} = U_{i+2}, \quad E_{i2} = E_{i+2}, \tag{9a}$$

$$A_{i1j1} = A_{ij}, \quad A_{i1j2} = A_{i(j+2)}, \qquad A_{i2j2} = A_{(i+2)(j+2)}\,. \tag{9b}$$

Thus, equation (8) reduces to

$$M_i \frac{dU_i}{dt} = E_i - A_{ij}\frac{dU_j}{dt} - U_j(U_k - U_{k+2})\frac{\partial A_{ij}}{\partial s_k} + \frac{1}{2}\frac{\partial A_{jm}}{\partial s_k}(\delta_{ki} - \delta_{(k+2)i})\,U_j U_m \quad \text{(no sum on i)}, \tag{10}$$

where k = 1,2 and other subscripts have a range of 1 to 4, $M_1 = M_2$ is the mass of body 1 and $M_3 = M_4$ mass of body 2.

The added masses appearing in equation (10) are evaluated in the Cartesian coordinates shown in Fig. 1. For two bodies of revolution which are symmetric with respect to, and have their rotating axes perpendicular to, the xy-plane, the evaluation of added masses may be simplified significantly in another Cartesian coordinates (x', y'), where the x' axis is parallel to the line joining the centroids (Fig.2). In this new coordinate system, the translations of $o_1$ and $o_2$ can be decomposed into

components along the x' and y' axes and the new added masses $A'_{ij}$ (i, j = 1, 2, 3, 4), which are related to the centroidal or transversal motion of bobies, become functions of the separation distance s only. Since body 1 and body 2 are symmetric with respect to the centerline $o_1o_2$, a sign change in $U'_2$ should not change the fluid kinetic energy in terms of $A'_{ij}$. Therefore $A'_{12} = A'_{32} = 0$. Similarly, $A'_{14} = A'_{34} = 0$. Thus, the fluid kinetic energy T in this coordinate system is reduced to

$$2T = A'_{11}U'^2_{11} + 2A'_{13}U'_1U'_3 + A'_{33}U'^2_{33} + A'_{22}U'^2_{22} + 2A'_{24}U'_2U'_4 + A'_{44}U'^2_{44}. \tag{11}$$

Let $\gamma$ be the angle between the $x_1$ axis and the $x'_1$ axis (Fig.2). The transformation of velocities is given by

$$U'_i = b_{ij}\, U_j, \tag{12}$$

where $b_{ij}$ is the transformation tensor and its matrix representation is

$$\mathbf{B} = \begin{bmatrix} \cos\gamma & \sin\gamma & 0 & 0 \\ -\sin\gamma & \cos\gamma & 0 & 0 \\ 0 & 0 & \cos\gamma & \sin\gamma \\ 0 & 0 & -\sin\gamma & \cos\gamma \end{bmatrix}. \tag{13}$$

Zeros in **B** indicate that there is no constraint between body 1 and body 2. Based on the invariance of the kinetic energy to the coordinate transformation, we have

$$2T = A'_{ij}U'_iU'_j = A_{mn}\, U_mU_n,$$

where,

$$A_{mn} = A'_{ij}\, b_{im}\, b_{jn}. \tag{14a}$$

The added masses $A'_{ij}$ are functions of the separation distance s only, and $b_{ij}$ are functions of the angle $\gamma$. Equation (14) can also be expressed in matrix form as

$$\mathbf{A} = \mathbf{B}^T\, \mathbf{A}'\, \mathbf{B}, \tag{14b}$$

where $\mathbf{A} = [A_{ij}]$ and $\mathbf{A}' = [A'_{ij}]$ are matrices of added masses. By (13) and (14), we can explicitly write down the added masses $A_{ij}$ in terms of the added masses $A'_{ij}$ due to the centroidal and transversal motions with respect to the centerline. Thus

$$A_{11} = A'_{11}\cos^2\gamma + A'_{22}\sin^2\gamma, \qquad A_{13} = A'_{13}\cos^2\gamma + A'_{24}\sin^2\gamma,$$
$$A_{12} = (A'_{11} - A'_{22})\sin\gamma\cos\gamma, \qquad A_{14} = (A'_{13} - A'_{24})\sin\gamma\cos\gamma,$$
$$A_{22} = A'_{11}\sin^2\gamma + A'_{22}\cos^2\gamma, \qquad A_{23} = (A'_{13} - A'_{24})\sin\gamma\cos\gamma,$$
$$A_{34} = (A'_{33} - A'_{44})\sin\gamma\cos\gamma, \qquad A_{33} = A'_{33}\cos^2\gamma + A'_{44}\sin^2\gamma,$$
$$A_{24} = A'_{13}\sin^2\gamma + A'_{24}\cos^2\gamma, \qquad A_{44} = A'_{33}\sin^2\gamma + A'_{44}\cos^2\gamma, \tag{15}$$

The derivatives of added masses with respect to the k-th component of the separation distance $s_k$ (k=1, 2) are

$$\frac{\partial A_{mn}}{\partial s_k} = b_{im}\, b_{jn}\, \frac{\partial A'_{ij}}{\partial s}\frac{\partial s}{\partial s_k} + \left[\frac{\partial b_{im}}{\partial \gamma}\, b_{jn} + b_{im}\frac{\partial b_{jn}}{\partial \gamma}\right] A'_{ij}\frac{\partial \gamma}{\partial s_k}, \tag{16a}$$

or

$$\frac{\partial A_{11}}{\partial s_1} = \cos\gamma\frac{\partial A_{11}}{\partial s} - \frac{\sin\gamma}{s}\frac{\partial A_{11}}{\partial \gamma}, \qquad \frac{\partial A_{11}}{\partial s_2} = \sin\gamma\frac{\partial A_{11}}{\partial s} + \frac{\cos\gamma}{s}\frac{\partial A_{11}}{\partial \gamma}, \quad \text{etc.} \tag{16b}$$

where $s_1$ and $s_2$ are the components of $(\mathbf{x}_1 - \mathbf{x}_2)$ in the x and y directions respectively.

Equations of motion (10) have to be decoupled before we can solve them numerically. Let

$$\mathbf{G}(\mathbf{U}) = (U_1 - U_3)\,\mathbf{A}_{s_1} + (U_2 - U_4)\,\mathbf{A}_{s_2}, \tag{17}$$

where $\mathbf{A}_{s_k} = \partial\mathbf{A}/\partial s_k$ (k=1,2) are matrices formed by the derivatives of added masses (16), and $\mathbf{M}$ is a 4×4 diagonal matrix with elements $M_1, M_2, M_3, M_4$. Let $\mathbf{q}(\mathbf{U})$ be a column vector,

$$\mathbf{q}(\mathbf{U}) = \frac{1}{2}\,[\mathbf{U}^T\mathbf{A}_{s_1}\mathbf{U},\ \mathbf{U}^T\mathbf{A}_{s_2}\mathbf{U},\ -\mathbf{U}^T\mathbf{A}_{s_1}\mathbf{U},\ -\mathbf{U}^T\mathbf{A}_{s_2}\mathbf{U}]^T. \tag{18}$$

Then equation (10) may be written in vector form as

$$\frac{d\mathbf{U}}{dt} = (\mathbf{M} + \mathbf{A})^{-1}\,[\mathbf{E} - \mathbf{G}(\mathbf{U})\mathbf{U} + \mathbf{q}(\mathbf{U})], \tag{19}$$

where $\mathbf{E} = [E_1, E_2, E_3, E_4]^T$ is a column vector representing external forces acting on bodies 1 and 2. Replacing $\mathbf{U}$ by $(\mathbf{u} - \mathbf{U}_o)$, where $\mathbf{U}_o = [U_{o1}, U_{o2}, U_{o1}, U_{o2}]^T$, $U_{o1}$ and $U_{o2}$ are velocity components of the uniform flow in the x and y directions respectively, we obtain from (19) the equations of motion in the absolute coordinates.

$$\frac{\mathbf{du}}{\mathbf{dt}} = (\mathbf{M} + \mathbf{A})^{-1} [\mathbf{E} - \mathbf{G(u)u} + \mathbf{G(u)U_o} + \mathbf{q(u-U_o)}]. \tag{20}$$

There are various numerical techniques for solving the initial-value system presented by equation (20). In the present study, the Runge-Kutta-Fehlberg method, which was discussed in detail by Atkinson[14], are used for the solution of velocity components. The size of the time step is adaptive based on a pre-assigned error-control parameter in the calculation.

## III. EVALUATION OF ADDED MASSES AND THEIR DERIVATIVES

If the velocity potential due to the motion of solids can be represented by a set of isolated or distributed sigularities interior to solids, the well known Taylor's added-mass theorem and its generalization were recommended by Landweber and Yih[15] to determine the added masses. For a pair of three-dimensional solids moving in any manner in the xy-plane except pure rotations, the Taylor's added-mass formula can be generalized to (see Guo and Chwang[12])

$$A_{ij} + \delta_{ij} M'_j = 4\pi\rho \left[ \int_{V_j} -x_j \lambda_i dV + \sum (m_i x^o_j + \mu_{ij}) \right] \quad \text{(no sum on j)}, \tag{21}$$

where $M'_j$ is the mass of the fluid displaced by body 1 (for j = 1,2) or body 2 (for j = 3,4), $\lambda_i$ and $m_i$ are the volume-distributed source density and the isolated source strength, respectively, inside body j due to the i-th velocity component, $\mu_{ij}$ is the strength of an isolated dipole in the j-th direction inside body j associated with the i-th velocity component, $x_j$ and $x^o_j$ are the j-th local coordinate of $\lambda_i$ and $m_i$ respectively with respect to body j, the integration is over the volume of body j, $V_j$, and the summation is over all isolated singularities inside $V_j$.

In the case of centroidal motion of two spheres along their centerline, it is well known that the velocity potential of the fluid due to the unit motion of each sphere can be simply represented by a set of isolated doublets inside spheres. The location and strength of each doublet are determined by the sphere theorem which states that an isolated doublet of strength $\mu$ at a point P outside a sphere of radius a, pointing along the radial axis of the sphere, has its isolated-doublet image of strength $\mu(a/\lambda)^3$ at the inverse point inside the sphere with the direction opposite to the original one, where $\lambda$ ($\lambda$>a) is

the distance between the point P and the center of the sphere. Guo & Chwang[12] have discussed the strengths and locations of the image doublets for the motion of two cylinders and derived expressions of added masses and their derivatives by using Taylor's added-mass formula. With slight modification, their result can be extended to added masses and their derivatives due to centroidal motion of two spheres. By applying the Taylor's added-mass formula and the sphere theorem to the centroidal motion of two spheres, we have

$$A'_{11} = 4\pi\rho \left[ \sum_{n=0}^{\infty} \mu_{2n} - \frac{a^3}{3} \right], \qquad A'_{13} = 4\pi\rho \sum_{n=0}^{\infty} \mu_{2n+1},$$

$$A'_{33} = 4\pi\rho \left[ \sum_{n=0}^{\infty} \mu^*_{2n} - \frac{b^3}{3} \right], \qquad A'_{31} = A'_{13}, \tag{22}$$

where $\mu_{2n}$ is the strength of the n-th image doublet inside sphere 1 of radius a due to the unit motion of sphere 1 along the x' direction ($U'_1 = 1$, $U'_2 = U'_3 = U'_4 = 0$), $\mu_{2n+1}$ is the strength of the image doublet of $\mu_{2n}$ inside sphere 2 of radius b, $\mu^*_{2n}$ denotes the strength of the n-th image doublet inside sphere 2 due to the unit motion of sphere 2 in the x' direction ($U'_3 = 1$, $U'_1 = U'_2 = U'_4 = 0$), and $\rho$ is the density of the fluid. Analogous to the analysis of Guo & Chwang[12], we can show that sequences $\{\mu_{2n}\}$ and $\{\mu_{2n+1}\}$ are uniformly convergent for s in the region $[a+b,\infty)$, while their derivatives with respect to s are uniformly convergent in the region $(a+b,\infty)$ but divergent as s approaches (a+b). When $s > (a+b)$, the derivatives of added masses are given by

$$\frac{dA'_{11}}{ds} = 4\pi\rho \sum_{n=0}^{\infty} \frac{d\mu_{2n}}{ds}, \qquad \frac{dA'_{13}}{ds} = 4\pi\rho \sum_{n=0}^{\infty} \frac{d\mu_{2n+1}}{ds},$$

$$\frac{dA'_{33}}{ds} = 4\pi\rho \sum_{n=0}^{\infty} \frac{d\mu^*_{2n}}{ds}, \qquad \frac{dA'_{31}}{ds} = \frac{dA'_{13}}{ds}. \tag{23}$$

The general strengths and locations of image doublets and their derivatives with respect to s are determined by the iterative formula,

$$\mu_o = a^3/2, \qquad \frac{d\mu_o}{ds} = 0, \qquad \lambda_o = s, \qquad \frac{d\lambda_o}{ds} = 1,$$

$$\mu_{2n+1} = -\mu_{2n}\left(\frac{b^3}{\lambda_{2n}^3}\right), \qquad \frac{d\mu_{2n+1}}{ds} = -\frac{d\mu_{2n}}{ds}\left(\frac{b^3}{\lambda_{2n}^3}\right) + 3\mu_{2n}\left(\frac{b^3}{\lambda_{2n}^4}\right)\left(\frac{d\lambda_{2n}}{ds}\right),$$

$$\lambda_{2n+1} = s - \frac{b^2}{\lambda_{2n}}, \qquad \frac{d\lambda_{2n+1}}{ds} = 1 + \left(\frac{b^2}{\lambda_{2n}^2}\right)\left(\frac{d\lambda_{2n}}{ds}\right),$$

$$\mu_{2n+2} = -\mu_{2n+1}\left(\frac{a^3}{\lambda_{2n+1}^3}\right), \qquad \frac{d\mu_{2n+2}}{ds} = -\frac{d\mu_{2n+1}}{ds}\left(\frac{a^3}{\lambda_{2n+1}^3}\right) + 3\mu_{2n+1}\left(\frac{a^3}{\lambda_{2n+1}^4}\right)\left(\frac{d\lambda_{2n+1}}{ds}\right),$$

$$\lambda_{2n+2} = s - \frac{a^2}{\lambda_{2n+1}}, \qquad \frac{d\lambda_{2n+2}}{ds} = 1 + \left(\frac{a^2}{\lambda_{2n+1}^2}\right)\left(\frac{d\lambda_{2n+1}}{ds}\right), \tag{24}$$

where $\lambda_{2n}$ denotes the distance form $o_2$ to the n-th inverse point in sphere 1 and $\lambda_{2n+1}$that from $o_1$ to the (n+1)-th inverse point in sphere 2. All inverse points lie on the centerline $o_1o_2$. The value of $\mu^*_{2n}$ is obtained directly by interchanging a and b in equation (24). The limiting values of added masses, as s approaches (a+b), are derived as

$$\lim_{s\to(a+b)} A'_{11} = 4\pi\rho\left[\frac{a^3 b^3}{2(a+b)^3}\sum_{n=0}^{\infty}\frac{1}{\left(n + \frac{b}{a+b}\right)^3} - \frac{a^3}{3}\right], \tag{25a}$$

$$\lim_{s\to(a+b)} A'_{13} = -2\pi\rho\frac{a^3 b^3}{(a+b)^3}\zeta(3) = -2.10360\,\pi\rho\frac{a^3 b^3}{(a+b)^3}, \tag{25b}$$

where $\zeta(3)$ is the zeta function. As s tends to (a+b), however, the n-th terms of sequences $\{d\mu_{2n}/ds\}$ and $\{d\mu_{2n+1}/ds\}$ do not approach zero as n goes to infinity, and the derivatives of added masses are divergent. Thus, when two spheres are very close to each other, the kinetic energy of the fluid due to the centroidal motion of these two spheres is finite but the hydrodynamic interaction forces approach infinity.

When two spheres make transversal motion perpendicular to the centerline $o_1o_2$, the determination of the strengths and locations of the hydrodynamic singularities become very difficult. Consider the unit motion of sphere 1, $U'_2 = 1$, $U'_1 = U'_3 = U'_4 = 0$. If sphere 2 were absent, the velocity potential due to this motion could be represented by an isolated doublet located at $o_1$ in the direction of $U'_2$. However, the presence of sphere 2 violates the boundary condition on surface 2 and it requires images of the isolated doublet to satisfy the boundary condition. Since this doublet is

perpendicular to the radial axis of sphere 2, its images include an isolated doublet at the inverse point inside sphere 2 plus a line distribution of doublets from the inverse point to the center of sphere 2. The isolated and the line-distributed doublets in sphere 2 have another set of images in sphere 1, which include an isolated doublet at the inverse point and a more complicated line distribution of doublets from the inverse point to $o_1$. Very rapidly, the expression of image doublets in each sphere becomes extremely complicated. Hicks[2] stopped his calculation at the fourth image system because of the exceedingly laborious work and presented an approximation of the velocity potential due to the transversal motion when the separation distance s is considerably large.

In the present study, however, we shall consider directly the velocity potential of the fluid instead of the hydrodynamic singularities. Let us consider two sets of spherical coordinate systems $(r_1,\theta_1,\lambda_1)$ and $(r_2,\theta_2,\lambda_2)$ with origins located at $o_1$ and $o_2$ respectively, the common polar axis being $o_1o_2$ (see Fig. 3). Let $\phi^{(i)}$ be the velocity potential due to the unit motion of sphere 1 in the direction of $U'_2$ and expressed in terms of the i-th (i = 1,2) set of the spherical coordinate system. In the absence of sphere 2, $\phi_0^{(1)}$, the velocity potential due to the motion of sphere 1, would be the solution of the Laplace equation satisfying the boundary condition on surface 1. If sphere 2 is inserted into the field at $o_2$, we should add an extra term $\phi_1^{(2)}$ to the velocity potential $\phi_0^{(2)}$, which is $\phi_0^{(1)}$ expressed in the $(r_2,\theta_2,\lambda_2)$ coordinate system, in order to satisfy the boundary condition on surface 2. Thus, the new expression for the velocity potential around these two spheres becomes

$$\phi^{(2)} = \phi_0^{(2)} + \phi_1^{(2)}.$$

However, the added term $\phi_1^{(2)}$ violates the boundary condition on the surface 1 again and requires an additional term $\phi_2^{(1)}$ to satisfy the boundary condition on surface 1. Thus

$$\phi^{(1)} = \phi_0^{(1)} + \phi_1^{(1)} + \phi_2^{(1)}.$$

Continuing this process, we can determine the velocity potential due to the transversal motion of sphere 1 in the y' direction ($U'_2 = 1$, $U'_1 = U'_3 = U'_4 = 0$) as

$$\phi^{(1)} = \sum_{m=0}^{\infty} \phi_m^{(1)}, \tag{26a}$$

or

$$\phi^{(2)} = \sum_{m=0}^{\infty} \phi_m^{(2)}. \tag{26b}$$

In the spherical coordinates $(r_1, \theta_1, \lambda_1)$, $\phi^{(1)}$ satisfies the Laplace equation and the boundary condition on sphere 1,

$$(\nabla^{(1)})^2 \phi^{(1)} = 0, \qquad \frac{\partial \phi^{(1)}(a,\theta_1,\lambda)}{\partial r_1} = \sin\theta_1 \cos\lambda, \tag{27}$$

where $\lambda = \lambda_1 = \lambda_2$ and

$$(\nabla^{(i)})^2 = \frac{1}{r_i^2}\frac{\partial}{\partial r_i}\left(r_i^2 \frac{\partial}{\partial r_i}\right) + \frac{1}{r_i^2 \sin\theta_i}\frac{\partial}{\partial \theta_i}\left(\sin\theta_i \frac{\partial}{\partial \theta_i}\right) + \frac{1}{r_i^2 \sin^2\theta_i}\frac{\partial^2}{\partial \lambda^2} \qquad (i = 1,2)$$

are the Laplacian operator in $(r_i, \theta_i, \lambda)$. In the coordinates $(r_2, \theta_2, \lambda)$, $\phi^{(2)}$ satisfies

$$(\nabla^{(2)})^2 \phi^{(2)} = 0, \qquad \frac{\partial \phi^{(2)}(b,\theta_2,\lambda)}{\partial r_2} = 0. \tag{28}$$

Around sphere 1, the general solution of equation (27) is given by

$$\phi^{(1)} = \left[ -\frac{R_1}{r_1^2} + \sum_{n=1}^{\infty} A_n(s) R_n \left(r_1^n + \frac{n}{n+1}\frac{a^{2n+1}}{r_1^{n+1}}\right)\right] \frac{a^3}{2} \cos\lambda, \tag{29a}$$

and in the neighborhood of sphere 2, the solution of equation (28) is

$$\phi^{(2)} = \left(\frac{a^3}{2}\cos\lambda\right) \sum_{n=1}^{\infty} B_n(s) S_n \left(r_2^n + \frac{n}{n+1}\frac{b^{2n+1}}{r_2^{n+1}}\right), \tag{29b}$$

where $R_n = P_n^1(\cos\theta_1)$ is the associated Legendre function of degree n and of order 1, $S_n = P_n^1(\cos\theta_2)$, $A_n$ and $B_n$ are arbitary coefficients which depend on the separation distance s and should be determined by the boundary conditions on both surfaces.

The transformation of $R_n$ and $S_n$ in these two sets of spherical coordinate systems $(r_1, \theta_1, \lambda)$ and $(r_2, \theta_2, \lambda)$ will be used frequently in the following analysis. For the associated Legendre function of degree n and of order m, the general transformation was first given by Basset[16],

$$\frac{P_n^m(\cos\theta_1)}{r_1^{n+1}} = \frac{(-1)^{n-m} r_2^m}{(n-m)!\, s^{n+m+1}} \sum_{k=0}^{\infty} \frac{(n+m+k)!}{(2m+k)!} \left(\frac{r_2}{s}\right)^k P_{m+k}^m(\cos\theta_2), \tag{30a}$$

$$\frac{P_n^m(\cos\theta_2)}{r_2^{n+1}} = \frac{r_1^m}{(n-m)!\, s^{n+m+1}} \sum_{k=0}^{\infty} \frac{(-1)^k (n+m+k)!}{(2m+k)!} \left(\frac{r_1}{s}\right)^k P_{m+k}^m(\cos\theta_1). \tag{30b}$$

For m = 1, the transformation is simplified to

$$\frac{R_n}{r_1^{n+1}} = \frac{(-1)^{n-1}}{(n-1)!\, s^{n+1}} \sum_{k=1}^{\infty} \frac{(n+k)!}{(k+1)!} \left(\frac{r_2}{s}\right)^k S_k, \tag{31a}$$

$$\frac{S_n}{r_2^{n+1}} = \frac{1}{(n-1)!\, s^{n+1}} \sum_{k=1}^{\infty} \frac{(-1)^{k-1}(n+k)!}{(k+1)!} \left(\frac{r_1}{s}\right)^k R_k. \tag{31b}$$

By the ratio test, we obtain that for any fixed n, the radius of convergence of the summation in (31a) is $r_2 < s$ and that of the summation in (31b) is $r_1 < s$.

If sphere 2 were absent, from (30a), the velocity potential would be

$$\phi_0^{(1)} = -\frac{R_1}{r_1^2} \left(\frac{a^3}{2} \cos\lambda\right).$$

From the transformation (31a), $\phi_0^{(1)}$ can be expressed in the second coordinate system as

$$\phi_0^{(2)} = \left(\frac{a^3}{2} \cos\lambda\right) \sum_{n=1}^{\infty} \Lambda_n^{[1]} r_2^n S_n \,.$$

where $\Lambda_n^{[1]} = - s^{-(n+2)}$. By comparing the velocity potential $\phi_0^{(2)}$ with the general solution (29b), we should add the term

$$\phi_1^{(2)} = (\frac{a^3}{2}\cos\lambda) \sum_{n=1}^{\infty} \Lambda_n^{[1]} S_n \frac{n}{n+1} \frac{b^{2n+1}}{r_2^{n+1}}$$

to $\phi_0^{(2)}$ in order to satisfy the boundary condition on surface 2. Thus

$$\phi_0^{(2)} + \phi_1^{(2)} = (\frac{a^3}{2}\cos\lambda) \sum_{n=1}^{\infty} \Lambda_n^{[1]} S_n (r_2^n + \frac{n}{n+1} \frac{b^{2n+1}}{r_2^{n+1}}),$$

which is convergent as $r_2 < s$. The term $\phi_1^{(2)}$, which can be expressed in the first coordinate system as

$$\phi_1^{(1)} = (\frac{a^3}{2}\cos\lambda) \sum_{n=1}^{\infty} \Lambda_n^{[2]} r_1^n R_n,$$

where

$$\Lambda_n^{[2]} = (-1)^{n-1} \sum_{k=1}^{\infty} \frac{k^2 b^{2k+1} (n+k)!}{(n+1)! (k+1)! s^{n+k+1}} \Lambda_k^{[1]},$$

makes an extra contribution to the velocity potential and in turn violates the boundary condition on surface 1. This contribution should be corrected by adding $\phi_2^{(1)}$ to the velocity potential $\phi_1^{(1)}$ ,

$$\phi_1^{(1)} + \phi_2^{(1)} = (\frac{a^3}{2}\cos\lambda) \sum_{n=1}^{\infty} \Lambda_n^{[2]} R_n (r_1^n + \frac{n\, a^{2n+1}}{(n+1)\, r_1^{n+1}}),$$

which satisfies the boundary condition on sphere 1 but not on sphere 2. The summation is convergent as $r_1 < s$. Repeating the same process indefinitely, we obtain the velocity potential $\phi^{(1)}$ and $\phi^{(2)}$, given by (29a) and (29b) respectively, with the coefficients

$$A_n(s) = \sum_{m=0}^{\infty} \Lambda_n^{[2m]}, \qquad B_n(s) = \sum_{m=0}^{\infty} \Lambda_n^{[2m+1]}, \tag{32}$$

where

$$\Lambda_n^{[0]} = 0, \qquad \Lambda_n^{[1]} = -\, s^{-(n+2)},$$

$$\Lambda_n^{[2m]} = (-1)^{n-1} \sum_{k=1}^{\infty} \frac{k^2 b^{2k+1} (n+k)!}{(n+1)! (k+1)! s^{n+k+1}} \Lambda_k^{[2m-1]},$$

$$\Lambda_n^{[2m+1]} = \sum_{k=1}^{\infty} \frac{(-1)^{k-1} k^2 a^{2k+1} (n+k)!}{(n+1)!\,(k+1)!\, s^{n+k+1}} \Lambda_k^{[2m]} . \tag{33}$$

It can be shown that both $A_n(s)$ and $B_n(s)$ are less than $Cs^{-n}$, where C is a positive constant. Therefore, $\phi^{(1)}$ and $\phi^{(2)}$ are convergent uniformly in the neighborhood of sphere 1 and sphere 2 respectively.

By equations (7), (9), (27), and (29), and the relation $\phi^{(1)} = \phi^{(2)}$, we have

$$A'_{22} = -\frac{\rho a^5}{2} \int_0^{2\pi} \cos^2\lambda d\lambda \int_0^{\pi} \sin^2\theta_1 [ -\frac{R_1}{a^2} + \sum_{n=1}^{\infty} ( \sum_{m=0}^{\infty} \Lambda_n^{[2m]} ) \frac{2n+1}{n+1} a^n R_n ] d\theta_1$$

$$= \frac{1}{2} M'_1 (1 - \frac{3}{2} \sum_{m=0}^{\infty} \Lambda_1^{[2m]} a^3) . \tag{34a}$$

In the integration, all terms containing $R_n$, n>1, vanish because of the orthogonality relation. Similarly, $A'_{24}$, and $A'_{44}$ are given by

$$A'_{24} = -\frac{3\rho a^3 b^3}{4} \int_0^{2\pi} d\lambda \int_0^{\pi} \sin^2\theta_1 \cos^2\lambda \sum_{n=1}^{\infty} ( \sum_{m=0}^{\infty} \Lambda_n^{[2m+1]} ) S_1 d\theta_1 = -\frac{3a^3 M'_2}{4} \sum_{m=0}^{\infty} \Lambda_1^{[2m+1]}, \tag{34b}$$

$$A'_{44} = -\frac{b^5 \rho}{2} \int_0^{2\pi} d\lambda \int_0^{\pi} \sin^2\theta_2 \cos^2\lambda [ -\frac{S_1}{b^2} + \sum_{n=1}^{\infty} ( \sum_{m=0}^{\infty} \Lambda_n^{*[2m]} ) \frac{2n+1}{n+1} b^n S_n ] d\theta_2$$

$$= \frac{1}{2} M'_2 ( 1 - \frac{3b^3}{2} \sum_{m=0}^{\infty} \Lambda_1^{*[2m]} ). \tag{34c}$$

where $\Lambda_n^{*[2m]}$ are calculated by interchanging a and b in the iterative formula (33).

The derivatives of added masses with respect to the separation distance s are simply given by

$$\frac{dA'_{22}}{ds} = -\frac{3M'_1 a^3}{4} \sum_{m=0}^{\infty} \frac{d\Lambda_1^{[2m]}}{ds} , \qquad \frac{dA'_{24}}{ds} = -\frac{3 M'_2 a^3}{4} \sum_{m=0}^{\infty} \frac{\Lambda_1^{[2m+1]}}{ds} ,$$

$$\frac{dA'_{44}}{ds} = -\frac{3M'_2b^3}{4}\sum_{m=0}^{\infty}\frac{d\Lambda_1^{*[2m]}}{ds}. \tag{35}$$

From formula (33), the derivatives of $\Lambda_n^{[2m]}$ and $\Lambda_n^{[2m+1]}$ with respect to s are

$$\frac{d\Lambda_n^{[0]}}{ds} = 0, \qquad \frac{d\Lambda_n^{[1]}}{ds} = (n+2)\, s^{-(n+3)},$$

$$\frac{d\Lambda_n^{[2m]}}{ds} = (-1)^{n-1}\sum_{k=1}^{\infty}\frac{k^2b^{2k+1}(n+k)!}{(n+1)!(k+1)!}\left[\frac{1}{s^{n+k+1}}\frac{d\Lambda_k^{[2m-1]}}{ds} - \frac{(n+k+1)\Lambda_k^{[2m-1]}}{s^{n+k+2}}\right],$$

$$\frac{d\Lambda_n^{[2m+1]}}{ds} = \sum_{k=1}^{\infty}\frac{(-1)^{k-1}k^2a^{2k+1}(n+k)!}{(n+1)!(k+1)!}\left[\frac{1}{s^{n+k+1}}\frac{d\Lambda_k^{[2m]}}{ds} - \frac{(n+k+1)\,\Lambda_k^{[2m]}}{s^{n+k+2}}\right]. \tag{36}$$

We shall define the added-mass coefficients by

$$k_{ij} = A'_{ij} / M'_2 . \tag{37}$$

For the centroidal and transversal motions of two equal spheres, a/b = 1, the values of $k_{ij}$ are given in Table 1 with the separation distance s varying form 2.01 to 10.

## IV. NUMERICAL SOLUTION OF ADDED MASSES

In order to extend the above-mentioned analysis for a pair of spheres to the general case of two bodies of revolution, we may have recourse to the numerical computation of added masses, since the exact formulas such as equation (34) do not exist in general. In a given geometric and kinematic state, the Neumann boundary-value problem of two bodies needs to be solved numerically for either the velocity potential or the strengths of the surface distribution of sources on each body. We shall formulate the problem by the well-known boundary-integral method, which leads to a pair of Fredholm integral equations of the second kind, and consider the reliability of numerical solutions obtained from different procedures.

## IV.1 Formulation of integral equations

The boundary-integral method, derived from the generalized Taylor's formula and the fundamental relations between normal velocities and velocity potentials on solid surfaces, has been studied intensively by Landweber and Chwang[10]. Guo and Chwang[12] applied their treatment to a pair of two-dimensional cylinders and modified the integral equations for accurate solutions. For a pair of three-dimensional bodies translating in an unbounded fluid, the surface source distributions E(P') at point P' on surface 1 and F(Q') at point Q' on surface 2 are governed by the integral equations

$$2\pi E(P) - \int_{S_1} E(P') \frac{\partial}{\partial N_1} \frac{1}{R_{11}} dS - \int_{S_2} F(Q') \frac{\partial}{\partial N_1} \frac{1}{R_{21}} dS = U'_1 \frac{\partial x}{\partial N_1} + U'_2 \frac{\partial y}{\partial N_1}, \tag{38a}$$

$$2\pi F(Q) - \int_{S_1} E(P') \frac{\partial}{\partial N_2} \frac{1}{R_{12}} dS - \int_{S_2} F(Q') \frac{\partial}{\partial N_2} \frac{1}{R_{22}} dS = U'_3 \frac{\partial x}{\partial N_2} + U'_4 \frac{\partial y}{\partial N_2}, \tag{38b}$$

where $R_{ij}$ is the distance between the source point on body i and the field point on the surface of body j (i,j =1,2), $N_i$ denotes distance in the outward normal direction at the field point on the surface of body i. The terms $2\pi E(P)$ in (38a) and $2\pi F(Q)$ in (38b) appear after differentiating the singular integrals. As long as two bodies are separated, equations (38a,b) are well-defined at all points P and Q. However, there are two types of difficulties need to be considered in the numerical integrations:

1. There are apparent singularities involved in the kernels of the first integral in (38a) and of the second integral in (38b) when the point of integration coincides with the field point on the same surface. As discussed by Landweber and Chwang[10], the effect of apparent singularities can be reduced significantly by noting that the flux through a closed surface due to a unit source on the same surface is $2\pi$. For example, if there is a unit source at P on surface 1, then

$$- \int_{S_1} \frac{\partial}{\partial N'_1} \frac{1}{R_{11}} dS = 2\pi . \tag{39}$$

Thus, the first integral in (38a) can be modified as

$$-\int_{S_1} E(P')\frac{\partial}{\partial N_1}\frac{1}{R_{11}}dS = 2\pi E(P) - \int_{S_1}[E(P')\frac{\partial}{\partial N_1}\frac{1}{R_{11}} - E(P)\frac{\partial}{\partial N'_1}\frac{1}{R_{11}}]dS, \tag{40}$$

where the singularity at P' = P is eliminated.

2. There exist steep peak values in the kernels of the second integral in (38a) and of the first integral in (38b) when one body is in the proximity of the other and the point of integration is not on the same surface as that of the field point. Let $\delta$ be the gap distance between two surfaces, the maximum peak value of a typical kernel in the integral equations is of the order of $(1/\delta^2)$ for three-dimensional bodies. In order to remove the peaks, we may use a similar treatment to subtract a term from the integrand and then to add its accurate integration back to the equation. For example, the second integral in (38a) may be written as

$$\int_{S_2} F(Q')\frac{\partial}{\partial N_1}\frac{1}{R_{21}}dS = \int_{S_2}[F(Q')-F(Q_o)]\frac{\partial}{\partial N_1}\frac{1}{R_{21}}dS + F(Q_o)\int_{S_2}\frac{\partial}{\partial N_1}\frac{1}{R_{21}}dS\,, \tag{41}$$

in which $Q_o$ is the point where the maximum peak value occurs. The result of the integration on the left-hand side will be improved if the second integration on the right-hand side can be obtained exactly or computed more accurately without too much trouble. However, this modification has only weakened, rather than removed, the ill-behaved kernel since another peak value, whose magnitude is smaller than the original one, is still present in the first derivative of the kernel on the left-hand side. Depending on the smoothness of solid surfaces, this modification may be used successively[17].

The accuracy of the numerical solution for planar motion of two spheres will be examined by comparing it with the analytic solution. Let's define two spherical polar coordinate systems $(r_1, \alpha, \beta)$ and $(r_2, \theta, \delta)$ by (see Fig. 4)

$$\begin{aligned} x' &= r_1 \sin\alpha \cos\beta + s = r_2 \sin\theta \cos\delta, \\ y' &= r_1 \sin\alpha \sin\beta = r_2 \sin\theta \sin\delta, \\ z' &= r_1 \cos\alpha = r_2 \cos\theta. \end{aligned} \tag{42}$$

From equations (38), (40) and (41), the surface-source distribution on each spherical surface satisfies

the pair of integral equations

$$4\pi E(\alpha,\beta)-a^2\int_0^{2\pi}d\beta'\int_0^{\pi}[E(\alpha',\beta')-E(\alpha,\beta)]K_{11}(\alpha,\beta,\alpha',\beta')d\alpha'$$

$$-b^2\int_0^{2\pi}d\delta'\int_0^{\pi}[F(\theta',\delta')-F(0,\tfrac{\pi}{2})]K_{21}(\alpha,\beta,\theta',\delta')d\theta'$$

$$=b^2F(0,\tfrac{\pi}{2})\int_0^{2\pi}d\delta'\int_0^{\pi}K_{21}(\alpha,\beta,\theta',\delta')d\theta' + U'_1\cos\beta\sin\alpha+U'_2\sin\beta\sin\alpha, \qquad (43a)$$

$$4\pi F(\theta,\delta)-a^2\int_0^{2\pi}d\beta'\int_0^{\pi}[E(\alpha',\beta')-E(\pi,\tfrac{\pi}{2})]K_{12}(\theta,\delta,\alpha',\beta')d\alpha'$$

$$-b^2\int_0^{2\pi}d\delta'\int_0^{\pi}[F(\theta',\delta')-F(\theta,\delta)]K_{22}(\theta,\delta,\theta',\delta')d\theta'$$

$$=a^2E(\pi,\tfrac{\pi}{2})\int_0^{2\pi}d\beta'\int_0^{\pi}K_{12}(\theta,\delta,\alpha',\beta')d\alpha'+U'_3\cos\delta\sin\theta+U'_4\sin\delta\sin\theta. \qquad (43b)$$

Define

$$R(\xi,\eta,\zeta\,;\,x,y,z) = [(\xi - x)^2 + (\eta - y)^2 + (\zeta - z)^2]^{1/2},$$

then the distance $R_{ij}$ between the source point on body i and the field point on body j is (Fig.4)

$$R_{11}= (s+a\sin\alpha'\cos\beta',\ a\sin\alpha'\sin\beta',\ a\cos\alpha';\ s+a\sin\alpha\cos\beta,\ a\sin\alpha\sin\beta,\ a\cos\alpha),$$

$$R_{21}= (b\sin\theta'\cos\delta',\ b\sin\theta'\sin\delta',\ b\cos\theta';\ s+a\sin\alpha\cos\beta,\ a\sin\alpha\sin\beta,\ a\cos\alpha),$$

$$R_{12}= (s+a\sin\alpha'\cos\beta',\ a\sin\alpha'\sin\beta',\ a\cos\alpha';\ b\sin\theta\cos\delta,\ b\sin\theta\sin\delta,\ b\cos\theta),$$

$$R_{22}= (b\sin\theta'\cos\delta',\ b\sin\theta'\sin\delta',\ b\cos\theta';\ b\sin\theta\cos\delta,\ b\sin\theta\sin\delta,\ b\cos\theta), \qquad (44)$$

where s is the separation distance between two spheres, $s = o_1o_2$. The kernel functions in the integral equations (43a,b) are given explicitly by

$$K_{11}(\alpha,\beta,\alpha',\beta') = -\frac{\sin\alpha'}{2^{3/2}\,a^2\,(1-\sin\alpha\sin\alpha'\cos(\beta-\beta') - \cos\alpha\cos\alpha')^{1/2}},$$

$$K_{21}(\alpha,\beta,\theta',\delta') = -\frac{1}{R_{21}^3}\sin\theta'[a-b\sin\theta'\sin\alpha\cos(\delta'-\beta)-b\cos\theta'\cos\alpha+s\sin\alpha\cos\beta],$$

$$K_{12}(\theta,\delta,\alpha',\beta') = -\frac{1}{R_{12}^3}\sin\alpha'[b-a\sin\alpha'\sin\theta\cos(\beta'-\delta)-a\cos\alpha'\cos\theta-s\sin\theta\cos\delta],$$

$$K_{22}(\theta,\delta,\theta',\delta') = -\frac{\sin\theta'}{2^{3/2}\,b^2\,(1-\sin\theta\sin\theta'\cos(\delta-\delta')-\cos\theta\cos\theta')^{1/2}}. \tag{45}$$

In the derivation of equations (43a,b), we have used the identity (39) and the relation for the i-th sphere

$$\frac{\partial}{\partial N_i}\left(\frac{1}{R_{ii}}\right) = \frac{\partial}{\partial N_i'}\left(\frac{1}{R_{ii}}\right). \tag{46}$$

Based on surface-source distributions obtained from integral equations (43a,b), we can compute the added-mass coefficients due to the motion of each sphere by means of equation (37) and the generalized Taylor's formula (21). For $U'_1 = 1$, $U'_2=U'_3=U'_4=0$,

$$k_{11} = \frac{a^3}{b^3}\left(3\int_0^{2\pi}d\beta\int_0^{\pi}E(\alpha,\beta)\sin^2\alpha\cos\beta\,d\alpha - 1\right), \tag{47a}$$

$$k_{13} = 3\int_0^{2\pi}d\delta\int_0^{\pi}F(\theta,\delta)\sin^2\theta\cos\delta\,d\theta. \tag{47b}$$

For $U'_2 = 1$, $U'_1=U'_3=U'_4=0$,

$$k_{22} = \frac{a^3}{b^3}\left(3\int_0^{2\pi}d\beta\int_0^{\pi}E(\alpha,\beta)\sin^2\alpha\sin\beta\,d\alpha - 1\right), \tag{47c}$$

$$k_{24} = 3\int_0^{2\pi}d\delta\int_0^{\pi}F(\theta,\delta)\sin^2\theta\sin\delta\,d\theta. \tag{47d}$$

Similarly, for $U'_3=1$, $U'_1=U'_2=U'_4=0$,

$$k_{33} = 3\int_0^{2\pi}d\delta\int_0^{\pi}F(\theta,\delta)\sin^2\theta\cos\delta\,d\theta - 1. \tag{47e}$$

Finally, for $U'_4=1$, $U'_1=U'_2=U'_3=0$,

$$k_{44} = 3 \int_0^{2\pi} d\delta \int_0^{\pi} F(\theta,\delta) \sin^2\theta \sin\delta \, d\theta - 1. \tag{47f}$$

As explained in deriving equation (11), we have

$$k_{12} = k_{23} = 0, \; k_{14} = k_{34} = 0. \tag{47g}$$

### IV.2 Numerical solutions of integral equations

The unknown source distributions $E(\alpha,\beta)$ and $F(\theta,\delta)$ for two spheres are governed by a set of two integral equations (43a,b). These equations will be transformed into two sets of linear equations by introducing appropriate quadrature formulas for the integrals, and solved by the Gauss-Seidel iterative method. Thus, for the (n+1)-th iteration, we have

$$4\pi E_{ij}^{n+1} - a^2 \sum_{i'} \sum_{j'} W_{1i'} W_{2j'} [E_{i'j'}^{n} - E_{ij}^{n}] K_{11iji'j'} - b^2 \sum_{k'} \sum_{m'} \Omega_{1k'} \Omega_{2m'} [F_{k'm'}^{n} - F_{o}^{n}] K_{21ijk'm'}$$
$$= b^2 F_o^n \sum_{k'} \sum_{m'} \Omega_{1k'} \Omega_{2m'} K_{21ijk'm'} + U'_1 \cos\beta \sin\alpha + U'_2 \sin\beta \sin\alpha, \tag{48a}$$

$$4\pi F_{km}^{n+1} - a^2 \sum_{i'} \sum_{j'} W_{1i'} W_{2j'} [E_{i'j'}^{n+1} - E_{o}^{n+1}] K_{12kmi'j'} - b^2 \sum_{l'} \sum_{m'} \Omega_{1k'} \Omega_{2m'} [F_{k'm'}^{n} - F_{km}^{n}] K_{22kmk'm'}$$
$$= a^2 E_o^{n+1} \sum_{i'} \sum_{j'} W_{1i'} W_{2j'} K_{12kmi'j'} + U'_3 \cos\delta \sin\theta + U'_4 \sin\delta \sin\theta, \tag{48b}$$

where W, $\Omega$ are weighting factors corresponding to different quadrature formulas, subscripts i, j, k, m refer to the location of a field point along $\alpha$, $\beta$, $\theta$, $\delta$ directions respectively, i', j', k', m' refer to that of a source point, and the superscript n stands for the n-th iteration. To start the numerical iteration process, we assume that the first approximation is

$$E_{ij}^{1} = (U'_1 \cos\beta \sin\alpha + U'_2 \sin\beta \sin\alpha)/4\pi \tag{49a}$$

and

$$F_{km}^{1} = (U'_3 \cos\delta \sin\theta + U'_4 \sin\delta \sin\theta)/4\pi. \tag{49b}$$

In fact, based on the numerical results, equations (48a) and (48b) always converge to the correct solution regardless of the initial approximation (49).

When two spheres are close to each other, it is evident that the source distribution on each surface changes rapidly around the gap between two surfaces. A typical distribution of $E(\alpha,\beta)$ for the case where $U'_1 = 1$, $U'_2 = U'_3 = U'_4 = 0$, and a/b = 1.0, s/b = 2.03 is shown in Figure 5 . To obtain an accurate numerical integration over the spherical surface, we shall put more node points near the gap by subdividing the region of integration into few partitions and apply the Gaussian quadrature formula in each subregion. The sizes of partitions measured by $\omega_\alpha$, $\omega_\beta$, etc. (Fig.6) are dependent on the separation distance s of two spheres. It is well known that most quadrature formulas, including the Gaussian quadrature formula, performs the best when the ill-behaved point is at the boundary of the integration region. In solving the integral equations (48a,b), however, we need to fix the field points as well as the point of integration on each surface in order to iterate the unknown source distributions. Thus, to compute the integrations on the right-hand sides of (43a,b) accurately, we shall rotate the coordinates in such a way that for each fixed field point on one surface, the maximum peak value on the other is always at the boundary of the integration region. Suppose that the peak of $K_{21}$, corresponding to a field point $P(a, \alpha_o, \beta_o)$ on sphere 1, occurs at $q(b, \theta^*, \delta^*)$ on sphere 2 (Fig. 7), then the integration of $K_{21}$ over surface 2 should be performed in the (X', Y', Z') coordinate system which is obtained by first rotating the (x', y', z') coordinate system about the z' axis with an angle $\delta^*$, then rotating about the new y' axis with an angle $(\frac{\pi}{2} - \theta^*)$. Therefore,

$$\mathbf{x}' = \mathbf{T}\,\mathbf{X}', \tag{50a}$$

where

$$\mathbf{T} = \begin{bmatrix} \cos\delta^*\sin\theta^* & -\sin\delta^* & -\cos\delta^*\cos\theta^* \\ \sin\delta^*\sin\theta^* & \cos\delta^* & -\sin\delta^*\cos\theta^* \\ \cos\theta^* & 0 & \sin\theta^* \end{bmatrix}. \tag{50b}$$

With this coordinate transformation, the first and the last abscissas for the Gaussian quadrature formulas in both $\theta$ and $\delta$ directions are in the nearest neighbourhood of q.

However, the explicit expression for point q in terms of $\alpha_o$ and $\beta_o$ is complicated so that we may have recourse to an approximation. It is noted that the peak affects the numerical integration significantly only in a region when the gap between two spheres are very small and the field point is

around the centerline (Fig. 7). In this region, the location of $q_o$, which is on the line of $Po_2$ (Fig. 7), should be very close to q, where the peak value of $K_{21}$ takes place. Thus

$$K_{21} = -\left(\frac{\sin\theta'}{R_{21}^2}\right)\cos(\pi-\psi) \approx \frac{(1-\psi^2/2)\sin\theta'}{R_{21}^2}, \qquad (\psi << 1).$$

We may examine the above-mentioned improvement by considering the following integral over sphere 2:

$$I = \int_0^{2\pi} d\delta' \int_0^{\pi} \frac{\sin\theta'}{R_{21}^2} d\theta' = -\frac{2\pi}{b\ d} \ln\left(\frac{d-b}{d+b}\right), \qquad (51)$$

where $d = |Po_2|$ (Fig.7). In this integration, the position of the source point q is exactly on the line $Po_2$. The analytical and numerical results of the integration I are plotted in Fig. 8, where we note that the deviation of the modified numerical result from the exact one is much smaller than that corresponding to the unmodified numerical result. Applying the modification (50) to equation (48a,b) and by means of (47), we can compute the added-mass coefficients. When $a/b = 1.0$ and s varies from 2.02 to 10, the numerical results of added-mass coefficients are listed in Table 2.

## V. DISCUSSION OF NUMERICAL RESULTS

The Lagrange's equations of motion, associated with the expression of kinetic energy of the fluid due to the planar translation of two bodies of revolution, can be applied to determine the hydrodynamic interaction between two bodies, as long as the flow is a potential flow. To solve equations (10) explicitly, we shall start the computation at the initial position $x_{io}$ (i=1, 2, 3, 4) with the initial absolute velocity components $u_{io}$ and the external forces $E_i$. At the beginning of the j-th time interval $\delta t_j$ (j = 1, 2, ...), the absolute velocities $u_{ij}$ are obtained by the fifth-order Runge-Kutta integration in terms of velocities in the previous time interval, $u_{ij-1}$, and the added masses and their derivatives evaluated at $x_{ij}$. At the end of the j-th time interval, the new position of each body is simply calculated by $x_{ij} = x_{ij-1} + u_{ij}\delta t_j$. The size of $\delta t_j$ is adaptive according to the value of a pre-assigned error-control parameter ($1.0*10^{-5}$) and the difference between the fifth- and the sixth-order

Runge-Kutta integration of $u_{ij}$. This process is repeated until either two bodies are in contact or one body passes over the other.

There are a number of real geometrical situations in which one can apply the afore-mentioned mathematical model to predict the motion of solids. In the present study, both bodies are assumed to be spheres with radii a and b ($a \leq b$) for bodies 1 and 2 respectively. In addition, we shall normalize all lengths by b, $a/b \leq 1.0$ and $s/b > (1.0+a/b)$.

We first consider the motion of a spherical particle of radius a, conveyed by a uniform flow, around a large spherical body fixed in space. This problem has applications in the ice-coating process. With $a/b=0.1$, $x_{1o}/b = -20$, $x_{2o}/b = 0.1, 0.3$, etc., and $u_{1o}/U_o = 1.0$, $u_{2o}/U_o = 0.0$, where $U_o$ is the uniform flow in the x direction, the trajectories of the particle are plotted in Fig. 9a to 9e for different density ratios of the body to the fluid medium. Fig. 9a corresponds to the case of an ice particle moving in fresh water and Fig. 9e shows the same ice particle in an air flow. The ratios 2.0, 5.0, and 10.0 correspond to various fluid media and illustrate the change of trajectories with respect to the density ratio. From these figures, we observe that the motion of the particle is affected by its inertia, which prevents the particle from moving out of its straight path, and by the interaction with the second sphere, which bends the particle trajectory to a curved streamline. In the case of an ice particle carried by an air flow (Fig. 9e), the inertia effect is so predominant that the trajectories are almost straight lines, whereas for the same particle moving in water (Fig. 9a), the curvature of the trajectories becomes very large when two bodies are close to each other. This conclusion can also be drawn from the equations of motion (20), which indicate that the accelerations of the particle in both $x_1$ and $x_2$ directions are proportional to $(\rho_a+\rho)^{-1}$. In some physical problems, it is important to determine whether or not a drifting body, conveyed by a current, can impact with a fixed body. This physical property can be expressed by a "collection coefficient" E which is defined as the ratio of the critical initial position $x^*_{2o}$, below which the drifting body will impact with the fixed body, to the radius of the fixed body. Fig. 10 shows the result of the collection coefficient for a pair of spheres, $0.01 \leq a/b \leq 1$, in fluids of different densities. Moving bodies of very small size are not considered since the Reynolds number becomes quite small such that the inviscid-fluid theory is not applicable.

Regarding a floating body in sea water, on the other hand, we should consider the change of hydrodynamic interaction between an ice floe, idealized as a sphere, and a fixed spherical offshore-structure versus the size of the floating body. For $\rho_a/\rho = 0.89$, the trajectories of a floating sphere of radius a (a/b=0.5, 1.0) around a fixed sphere are shown in Fig. 11. Initially, the floating sphere moves with the uniform flow, $u_{1o}/U_o = 1.0$ and $u_{2o}/U_o = 0.0$. These trajectories are quite flat in comparison with the ones of a small body since the inertia effect of a large body predominates over the hydrodynamic interaction force due to the presence of a second body.

To illustrate the dependence of trajectories of a moving sphere on its size, we plot the velocity components $u_1/U_o$ and $u_2/U_o$ in Fig. 12, and the trajectories in Fig. 13, respectively, for a sphere of various radius ratios a/b from 0.1 to 1.0 around a fixed sphere of radius b. The initial conditions used in these two figures are $x_{1o}/b = -20$, $x_{2o}/b = 0.5$, $u_{1o}/U_o=1.0$, $u_{2o}/U_o= 0.0$, and a fixed density ratio $\rho_a/\rho=0.89$. When two bodies are close to each other, Fig. 12 shows slight differences on the velocity components due to the size variation, while Fig. 13 shows that for the same initial position, the trajectories of sphere 1 is almost independent of its size. In Fig. 13, only the trajectory for the sphere a/b=0.1 (dotted line) can reach the position $x_1 = 0$, which indicates that the small sphere passes over the fixed one. All other trajectories terminate at certain position $o_1^f$ at which the two spheres are in contact. This phenomenon can be understood by considering the added masses. The first terms of added masses in (22) and (34) and their derivatives in (23) and (35) are proportional to $a^3$. These terms are predominant when s is sufficiently large, while the rest becomes significant only when s is very close to (a+b). Consequently, the predominant parts of the solution of equation (10) are almost independent of the radius a, since $a^3$ appears on both sides of (10). Based on this observation, we can surely use the trajectories for a small particle around a fixed blunt body as a good first approximation for the trajectories of a large body, or in some cases, we can even neglect the effect due to the size variation.

In the case of a small body pursuing a large target which moves in a fluid, we shall consider the influence of the motion of the target on the trajectories of the small body. Suppose that a large spherical target of radius b with $\rho_a/\rho = 0.89$ is initially located at (10,0) and moves in a stationary fluid

with $u_{3o}$=1.0, $u_{4o}$=0.0. A small particle of radius a (a/b=0.1) and density $\rho_a/\rho$=0.89 is released at (0, $x_{2o}$) with initial velocities $u_{1o}$ = 2.0 and $u_{2o}$ = ($x_{2o}$-1.1)/10. We can determine its trajectories based on the solution of (20). Without interaction, we would expect that these two bodies come in contact at x=20. However, from Fig.14, we note that the trajectories of the small particle are bent significantly in a region close to the large target due to the hydrodynamic interaction. This plot is consistent with the physical interpretation.

The magnitude and the direction of the hydrodynamic interaction force between two bodies depend on the relative motion between them and the direction of the oncoming flow. Fig. 15 shows the variation of the magnitude of the interaction force versus the flow direction and the separation distance. We note from Fig.15 that if the angle between the centerline and the flow direction is less than a certain value depending on the separation distance, the interaction force is repulsive, which prevents the collision of two bodies, whereas if the angle is larger than this value, the interaction force becomes attractive. Thus, when a particle moves towards the target sidewise from behind (see Fig. 14) and the angle between the centerline and the oncoming current is small, the interaction force repels the particle from the target and reduces its velocity component $u_2$. On the other hand, when the particle moves alongside of the target, the relative oncoming flow becomes almost perpendicular to the centerline, and the interaction force pushes the particle toward the target. This conclusion also indicates that if the angle between the centerline and the relative flow is large, the motion of the target generates an attractive force and the trajectory of the particle points toward the target without much bending (Fig.14, $x_{2o}/b$ = 4.0).

Another practical problem we shall consider in the present study is the hydrodynamic interaction between two bodies, idealized as spheres, when they move arbitrarily in a stationary fluid. Fig. 16 shows trajectories of two equal spheres (a/b = 1) with $\rho_a/\rho$ = 0.89, which corresponds to ice floes in sea water. Initially, both sphere move in a stationary fluid with velocities $u_1 = u_3 = 1$, $u_2 = u_4 = 0$, and the initial separation distance $s_o/b$ varies from 2.2 to 3.0. As we have discussed previously, the interaction force due to this type of motion attracts both bodies and drives them toward each other. The strength of the force, shown in Fig. 17 with a/b = 1 and $u_1 = u_3 = 1$, surely depend on the

separation distance s/b. The time required for two equal spheres to come into contact is shown in Fig. 18 versus the initial separation distance $s_o/b$. For $\rho_a/\rho = 0.89$ and a/b = 0.3, 0.5, 0.7, 1.0, Fig. 19 shows the trajectories of two spheres when they are initially released at $x_{1o} = x_{3o} = 0$ and $x_{2o} = -x_{4o} = 1.25b$ with velocities $u_{1o} = u_{3o} = 1$ and $u_{2o} = u_{4o} = 0$ in a stationary fluid. From this figure, we note that if sphere 1 is much smaller than sphere 2, its motion cannot affect the motion of sphere 2 significantly, since the inertia of sphere 2 is much larger than that of sphere 1. We also note that the variation of trajectories of sphere 1 due to the variation of the radius ratio a/b is much smaller than that for sphere 2, since the added masses associated with sphere 2 are more sensitive to the change of a/b.

## VI. CONCLUSIONS

A potential-flow prediction for the motion of a pair of bodies, and the hydrodynamic interaction force acting upon them in an inviscid fluid, have been presented. The Lagrange's equations of motion are generalized for planar translational motions of bodies, including the effects of solid constraints, external forces in the plane of motion, and a uniform stream in any direction parallel to the plane of motion. This generalization is applicable to bodies of revolution which are symmetric with respect to, and have their axes of rotation perpendicular to, the plane of motion. The velocity components and the moving trajectories of each body are obtained by integrating the equations of motion in terms of the kinetic energy of the fluid which is a function of added masses.

In order to determine the reliability of numerical solutions of interactions between a pair of three-dimensional solids, the exact solution of added masses and their derivatives in closed forms is first considered for the centroidal and transversal motions of two spheres. A new iterative formula has been developed to evaluate the added masses due to the transversal motion of two spheres based on the analysis of the velocity potential in the near field around the bodies. The added masses due to the centroidal motion are obtained by means of the Taylor's added-mass formula and an iterative scheme for the strengths and positions of interior doublets.

The boundary-integral method and the generalized Taylor's added-mass formula are used for numerical solutions of added masses. However, when two bodies are very close to each other, it is

difficult to obtain an accurate result because of the ill-behaved integral equations. These integral equations are modified by first subtracting out the steep peak value from the integration so that the resultant kernel is bounded, and then adding an accurate integration of the kernel back to the equation. As an example, the added masses of two equal spheres are computed numerically and the results are compared with exact solutions. A very good agreement has been obtained.

Due to the limitation of the potential-flow analysis, the afore-mentioned results are only applicable to cases where the effects of fluid inertia and the nonuniformity of the flow due to the presence of a second body are dominant.

## References


1. C. -C. Wu and L. Landweber, " Added Mass of Ogival Cylinders Oscillating Horizontally in a Free Surface, " Schiffstechnik, Vol. 7, No. 37, 1960.

2. Hicks. W. M., " On the Motion of Two Spheres in a Fluid," Proc. Trans. Roy. Soc. London, V. 171-II, 1880, 455-492.

3. Herman, R. A., "On the Motion of Two Spheres in Fluid and Allied Problems," Quart. J. Math, V. 22, 1887, 204-231.

4. Rouse, H. et. al., Advanced Mechanics of Fluids, Chapter 3, Robert E. Krieger Publishing Company, 1976.

5. Mitra, S. K., "A New Mehtod of Solution of the Boundary Value Problems of Laplace's Equation Relating to Two Spheres. - Part1", Bull. Calcutta Math. Soc., 36, 1944, 32-39.

6. Shail, R., "On Some Axisymmetrical Two Sphere Potential Problems", Mathematika 9, 1962, 57-70.

7. Atkinson, K. E., A Survey of umerical Methods for the Solution of Fredholm Integral Equations of the Second Kind, Society for Industrial and Applied Mathematics, Philadelphia, 1976.

8. Atkinson, K. E., "The Numerical Solution of Laplace's Equation in Three Dimensions", Society for Industrial and Applied Mathematics, 1982, 263-274.

9. Atkinson, K. E., " The Numerical Solution of Laplace's Equation in Three Dimensionas - II. Numerical Treatment of Integral Equations", J. Albrecht and L. Collatzeds., Birkhauser Verlag, Bassel, 1980, 1-23.

10. Landweber, L. and Chwang, A. T., "Generalization of Taylor's Added-Mass Formula for Two Bodies, " J. of Ship Research, Vol. 33, No.1, March 1989, 1-9.

11. Lamb, H., Hydrodynamics, 6th Ed., Chapter 6, Cambridge University Press. U. K., 1932.

12. Guo, Z. and Chwang, A. T., "Oblique Impact of Two Cylinders in a Uniform Flow," Submitted to J. of Ship Research, 1989.

13. Landweber, L., Chwang, A. T. and Guo, Z., "Interaction between Two Bodies Translating in an Inviscid Fluid," Submitted to the J. of Ship Research, 1989.

14. Atkinson, K. E., An Introduction to Numerical Analysis, Chapter 6, John Wiley & Sons. Inc., 1978.

15. Landweber, L. and Yih, C. S., "Forces, Moments, and Added Masses for Rankine Bodies", J. of Fluid Mechanics, Vol. 1, 1956, 319-336.

16. Basset, A. B., A Treaties on Hydrodynamics, Chapter XI, Dover Publications, Inc., 1961.

17. Melves, L. M. and Mohamed, J. L., Computational Methods for Integral Equations, Cambridge, 1985, Chapter 11.

Table 1. Exact Values of Added-Mass Coefficients for Two Equal Spheres (a/b = 1.0)

| s | $k_{11}$ | $-\frac{dk_{11}}{ds}$ | $-k_{13}$ | $\frac{dk_{13}}{ds}$ | $k_{22}$ | $-\frac{dk_{22}}{ds}$ | $-k_{24}$ | $\frac{dk_{24}}{ds}$ |
|---|---|---|---|---|---|---|---|---|
| 2.01 | 0.5702 | 0.5708 | 0.2163 | 0.7257 | 0.5191 | 0.1149 | 0.0984 | 0.2078 |
| 2.02 | 0.5651 | 0.4486 | 0.2097 | 0.6020 | 0.5180 | 0.1005 | 0.0964 | 0.1923 |
| 2.03 | 0.5610 | 0.3796 | 0.2041 | 0.5315 | 0.5171 | 0.0901 | 0.0945 | 0.1808 |
| 2.04 | 0.5575 | 0.3321 | 0.1990 | 0.4825 | 0.5162 | 0.0819 | 0.0927 | 0.1716 |
| 2.05 | 0.5543 | 0.2963 | 0.1944 | 0.4453 | 0.5154 | 0.0752 | 0.0911 | 0.1638 |
| 2.06 | 0.5515 | 0.2679 | 0.1901 | 0.4154 | 0.5147 | 0.0695 | 0.0895 | 0.1571 |
| 2.07 | 0.5490 | 0.2445 | 0.1861 | 0.3906 | 0.5140 | 0.0646 | 0.0879 | 0.1511 |
| 2.08 | 0.5466 | 0.2248 | 0.1823 | 0.3695 | 0.5134 | 0.0603 | 0.0864 | 0.1458 |
| 2.10 | 0.5425 | 0.1930 | 0.1752 | 0.3349 | 0.5123 | 0.0530 | 0.0836 | 0.1365 |
| 10.0 | 0.5000 | 0.0000 | 0.0015 | 0.0005 | 0.5000 | 0.0000 | 0.0008 | 0.0002 |

Table 2. Numerical Results of Added-Mass Coefficients for Two Equal Spheres (a/b = 1.0)

| s | $k_{11}$ | $-k_{13}$ | $k_{22}$ | $k_{24}$ | $\omega_\beta$ | $\omega_\alpha$ |
|---|---|---|---|---|---|---|
| 2.02 | 0.5614 | 0.2063 | 0.5182 | 0.0967 | 20 | 15 |
| 2.03 | 0.5591 | 0.2025 | 0.5171 | 0.0947 | 20 | 15 |
| 2.04 | 0.5562 | 0.1981 | 0.5162 | 0.0929 | 20 | 15 |
| 2.05 | 0.5540 | 0.1943 | 0.5154 | 0.0910 | 25 | 20 |
| 2.06 | 0.5512 | 0.1900 | 0.5147 | 0.0895 | 25 | 20 |
| 2.07 | 0.5486 | 0.1860 | 0.5140 | 0.0879 | 30 | 25 |
| 2.08 | 0.5464 | 0.1823 | 0.1534 | 0.0864 | 30 | 25 |
| 2.10 | 0.5421 | 0.1752 | 0.5123 | 0.0836 | 30 | 35 |
| 10.0 | 0.5000 | 0.0015 | 0.5000 | 0.0008 | 60 | 45 |

**Figure Captions**

Figure 1. Relative rectangular coordinate system (x, y, z) and velocity components.

Figure 2. Relative rectangular coordinate system (x', y', z') and velocity components.

Figure 3. Spherical polar coordinate systems ($r_1$, $\theta_1$, $\lambda_1$) and ($r_2$, $\theta_2$, $\lambda_2$).

Figure 4. Surface integration of source distributions on spheres 1 and 2.

Figure 5. Three-dimensional plotting of surface source distribution on sphere 1 with a/b = 1, s/b = 2.03, $U'_1$=1, and $U'_2$= $U'_3$= $U'_4$= 0.

Figure 6. Definition of regions containing peaks.

Figure 7. Rotation of the coordinate system (x', y', z') and definition sketch for d, $\alpha_o$, and $\beta_o$.

Figure 8. Comparison of numerical result of integral I (51) obtained with and without rotating coordinates.

Figure 9. Trajectories of a moving sphere in different fluids with a/b=0.1, $u_{1o}/U_o$=1, $u_{2o}/U_o$= 0, and $x_{1o}/b$ = -20.

Figure 10. Dependence of the collection coefficient E of an ice particle on the size for various density ratios.

Figure 11. Trajectories of a moving sphere with $x_{1o}/b$ = -20, $u_{1o}/U_o$=1, $u_{2o}/U_o$= 0, and $\rho_a/\rho$ = 0.89.

Figure 12. Velocity components $u_1$ and $u_2$ of a moving sphere with various radius ratios.

Figure 13. Trajectories of a moving sphere with various radius ratios.

Figure 14. Trajectories of a moving sphere with radius a affected by another sphere with radius b, a/b=0.1, $\rho_a/\rho$ = 0.89.

Figure 15. Dependence of interaction forces on the direction of a uniform flow.

Figure 16. Trajectories of two equal spheres (a/b=1) moving initially perpendicular to their centerline in a stationary fluid with $\rho_a/\rho$ = 0.89, a/b=1, $x_{1o}/b$ = $x_{3o}/b$ = 0, $u_{1o}$ =$u_{3o}$ = 1, and $u_{2o}$ =$u_{4o}$ = 0.

Figure 17. Interaction force between two equal spheres (a/b=1) versus the separation distance s/b.

Figure 18. Time required for two equal spheres (a/b=1) to come into contact versus the separation distance $s_o/b$ with $\rho_a/\rho$ = 0.89, $x_{1o}/b$ = $x_{3o}/b$ = 0, $u_{1o}$=$u_{3o}$= 1, and $u_{2o}$=$u_{4o}$= 0.

Figure 19. Trajectories of two spheres moving initially parallel to each other with $\rho_a/\rho$ = 0.89, $x_{1o}/b$ = $x_{3o}/b$ = 0, $x_{2o}/b$ = - $x_{4o}/b$ = 1.25, $u_{1o}$=$u_{3o}$= 1, and $u_{2o}$=$u_{4o}$= 0.

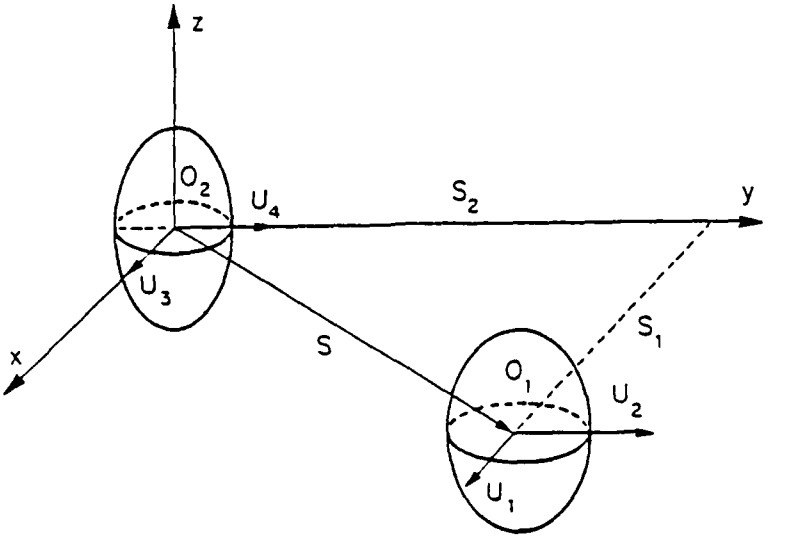


Figure 1. Relative rectangular coordinate system (x, y, z) and velocity components.

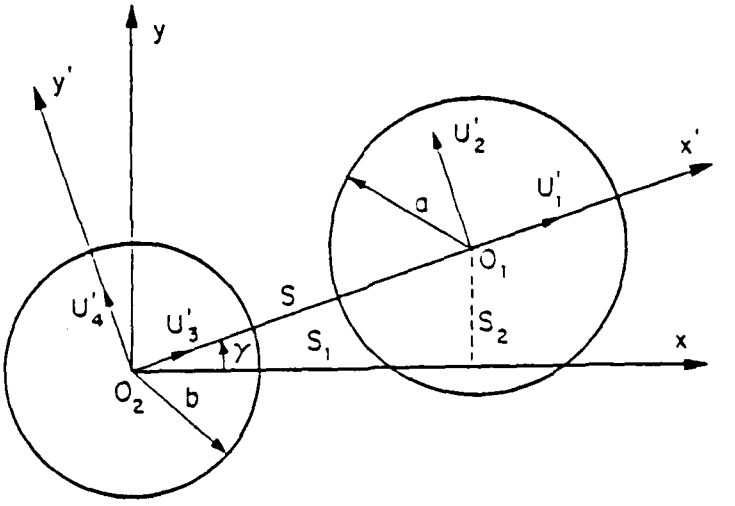


Figure 2. Relative rectangular coordinate system (x', y', z') and velocity components.

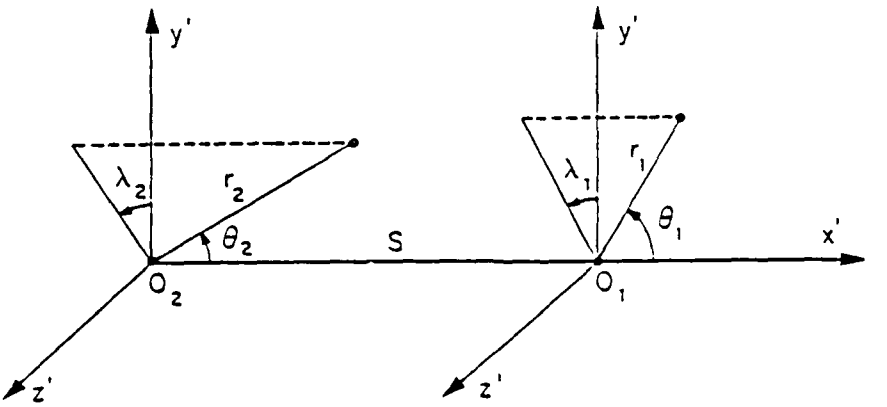


Figure 3. Spherical polar coordinate systems $(r_1, \theta_1, \lambda_1)$ and $(r_2, \theta_2, \lambda_2)$.

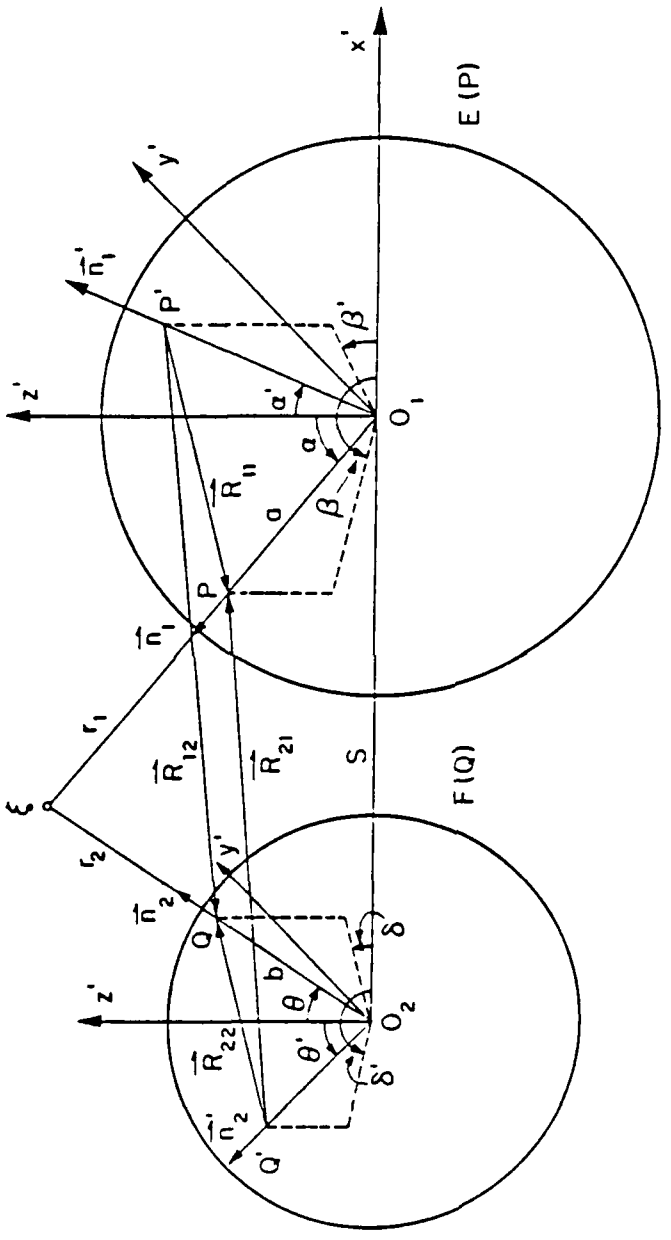


Figure 4. Surface integration of source distributions on spheres 1 and 2.

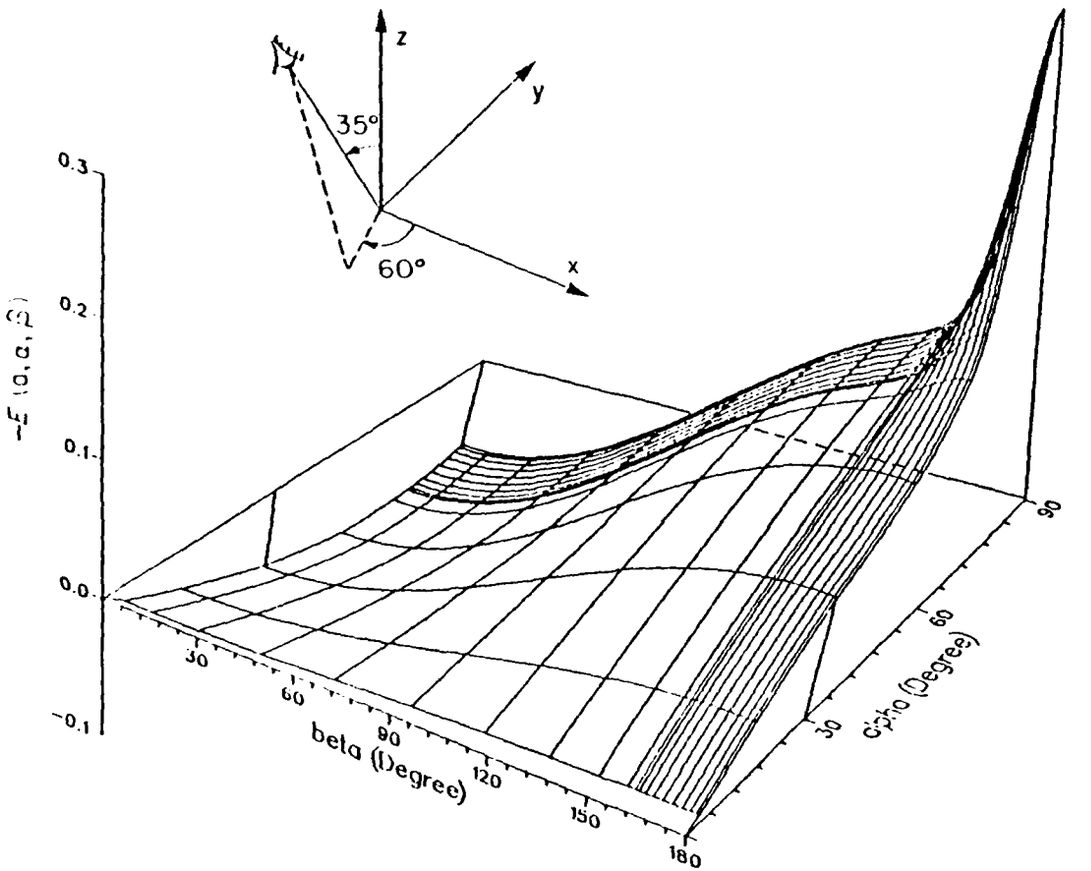


Figure 5. Three-dimensional plotting of surface source distribution on sphere 1 with a/b = 1, s/b = 2.03, $U'_1$=1, and $U'_2$= $U'_3$= $U'_4$= 0.

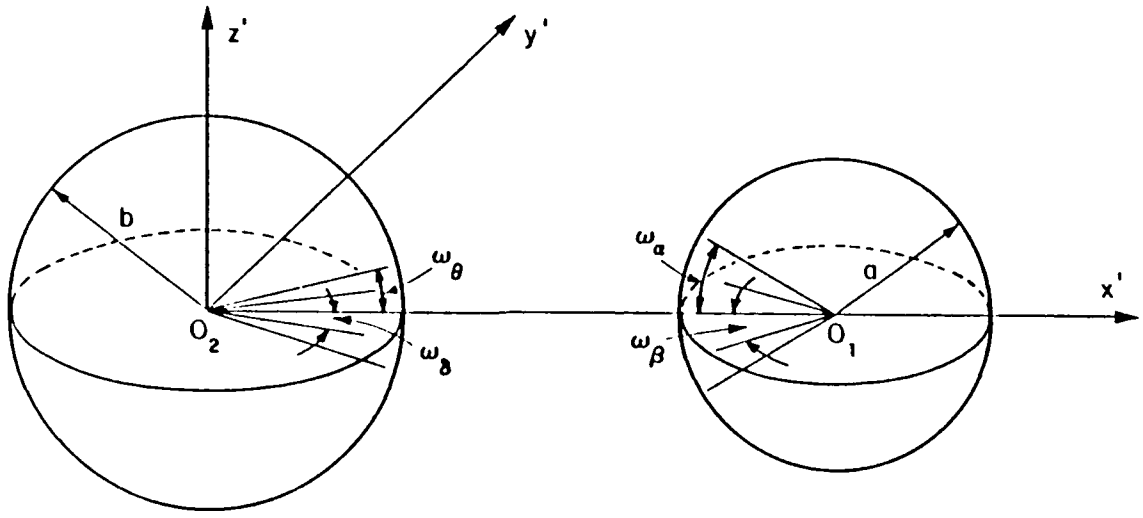


Figure 6. Definition of regions containing peaks.

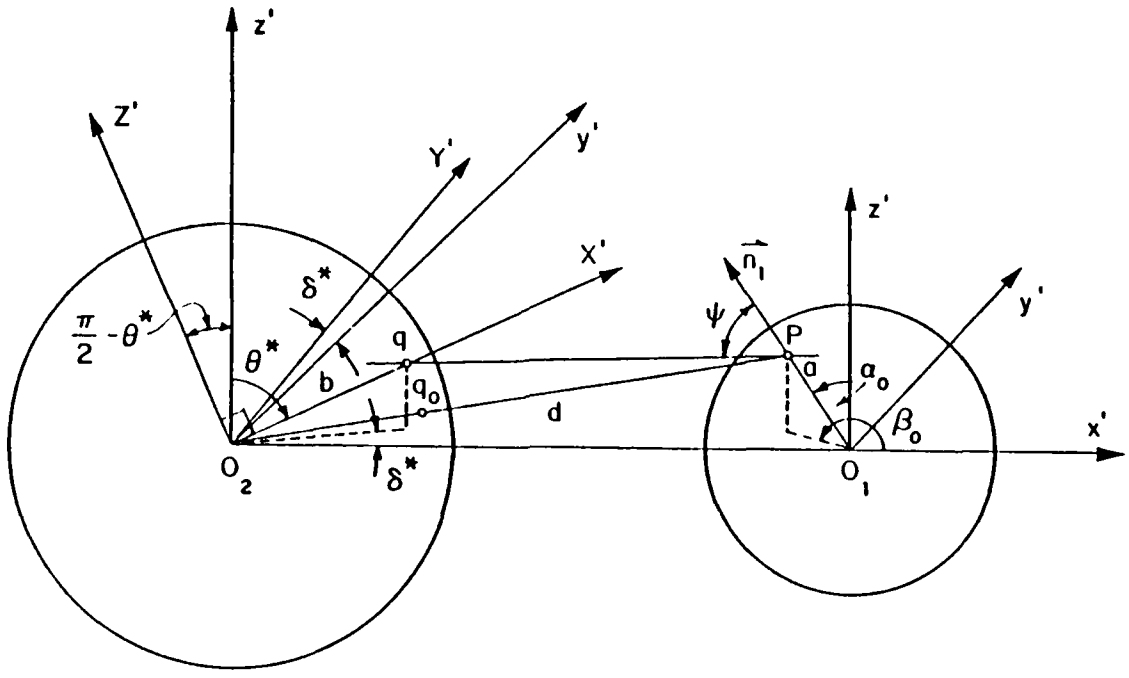


Figure 7. Rotation of the coordinate system (x', y', z') and definition sketch for d, $\alpha_0$, and $\beta_0$.

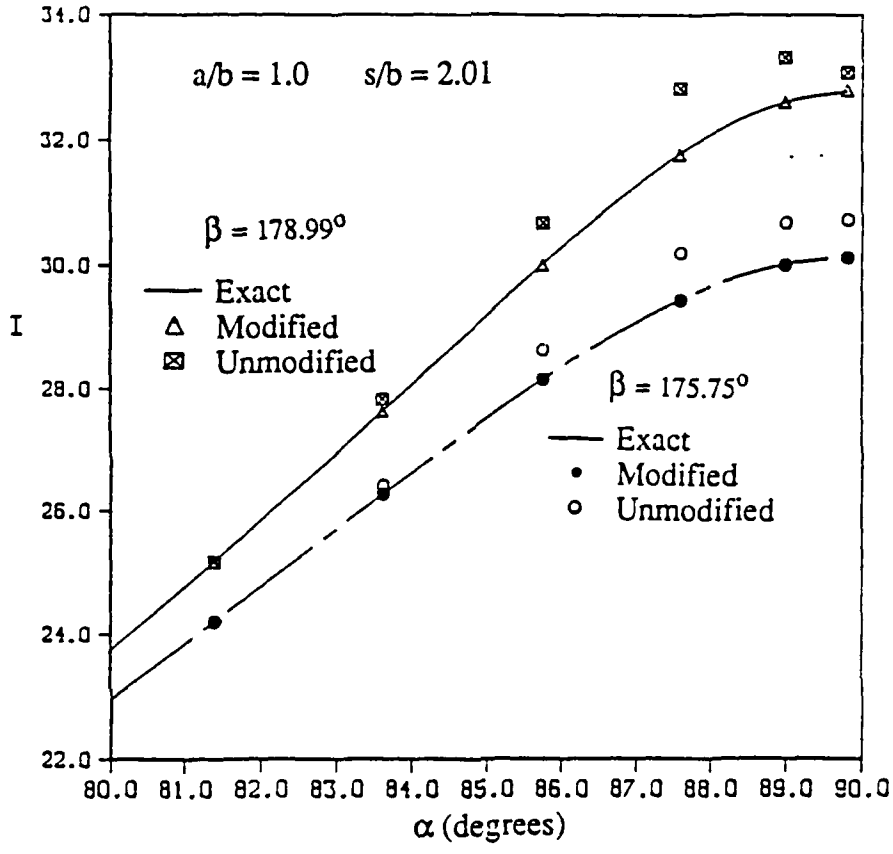


Figure 8. Comparison of numerical result of integral I (51) obtained with and without rotating coordinates.

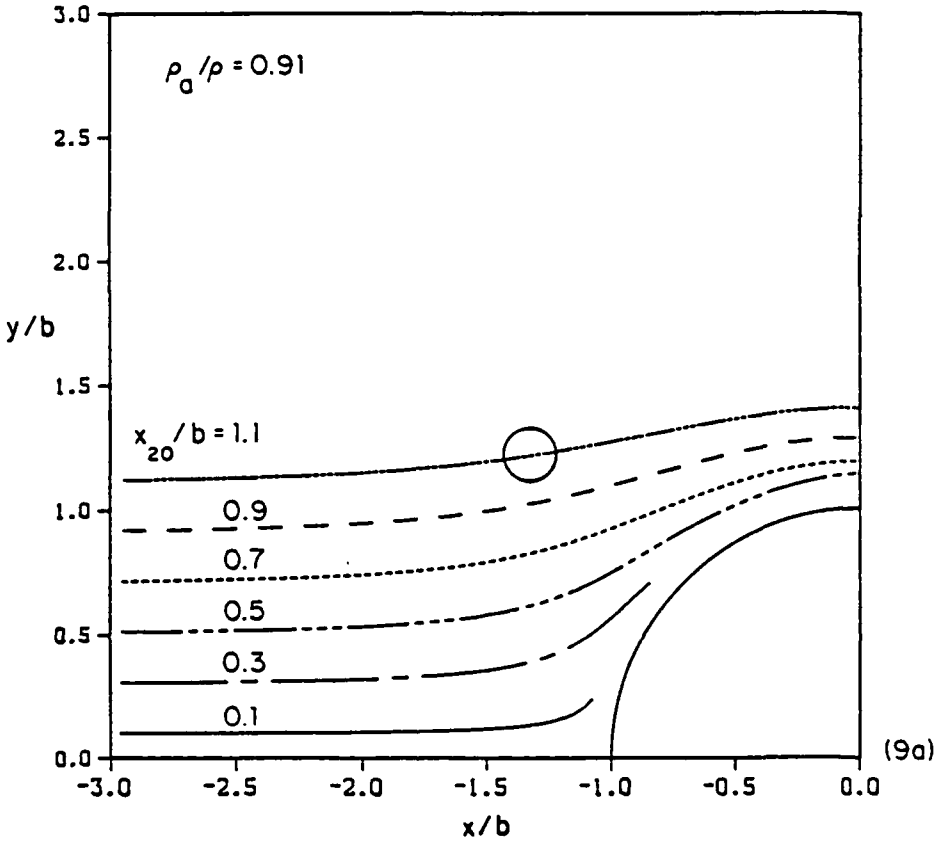


Figure 9. Trajectories of a moving sphere in different fluids with a/b=0.1, $u_{1o}/U_o$=1, $u_{2o}/U_o$= 0, and $x_{1o}/b$ = -20.

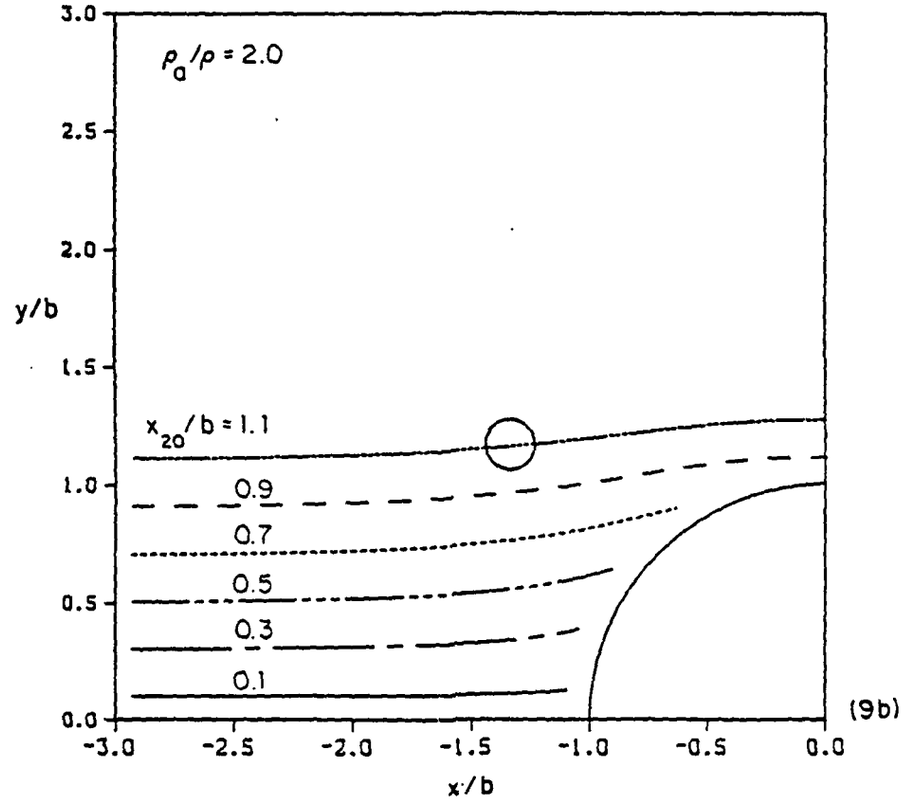


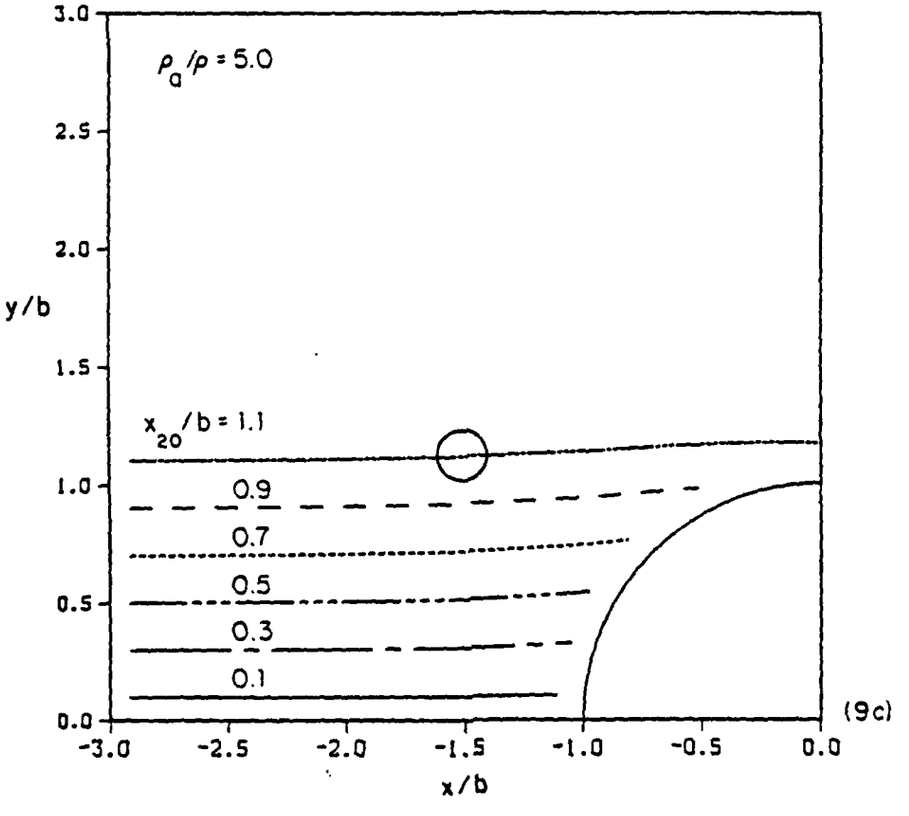


Figure 9. -- continued

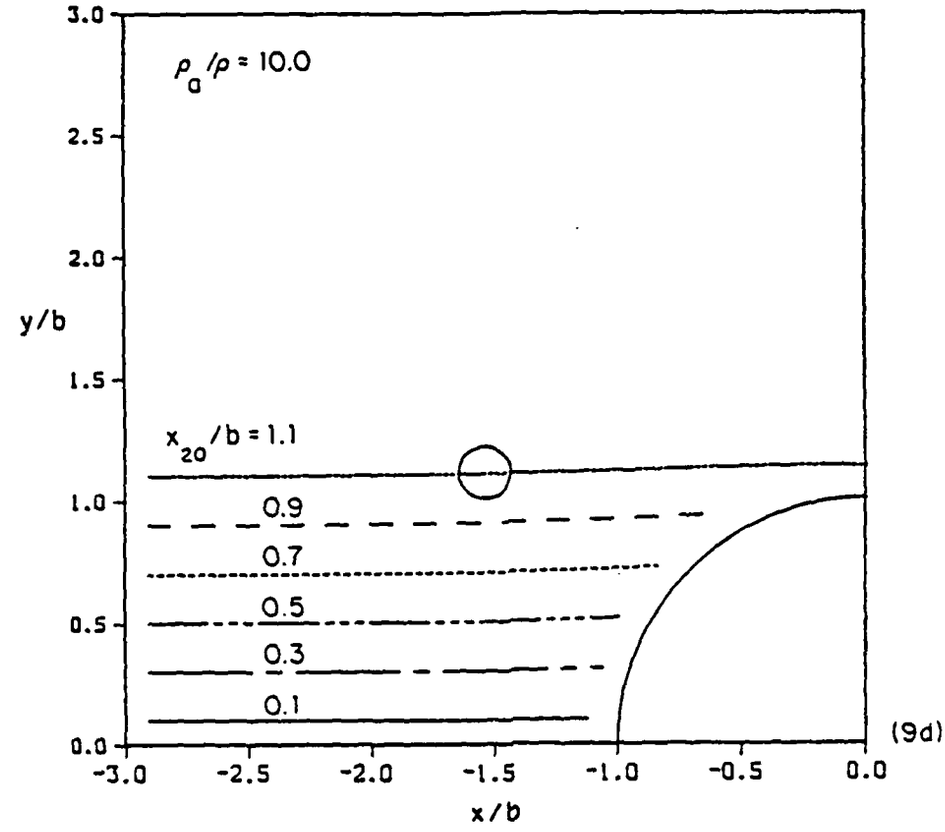


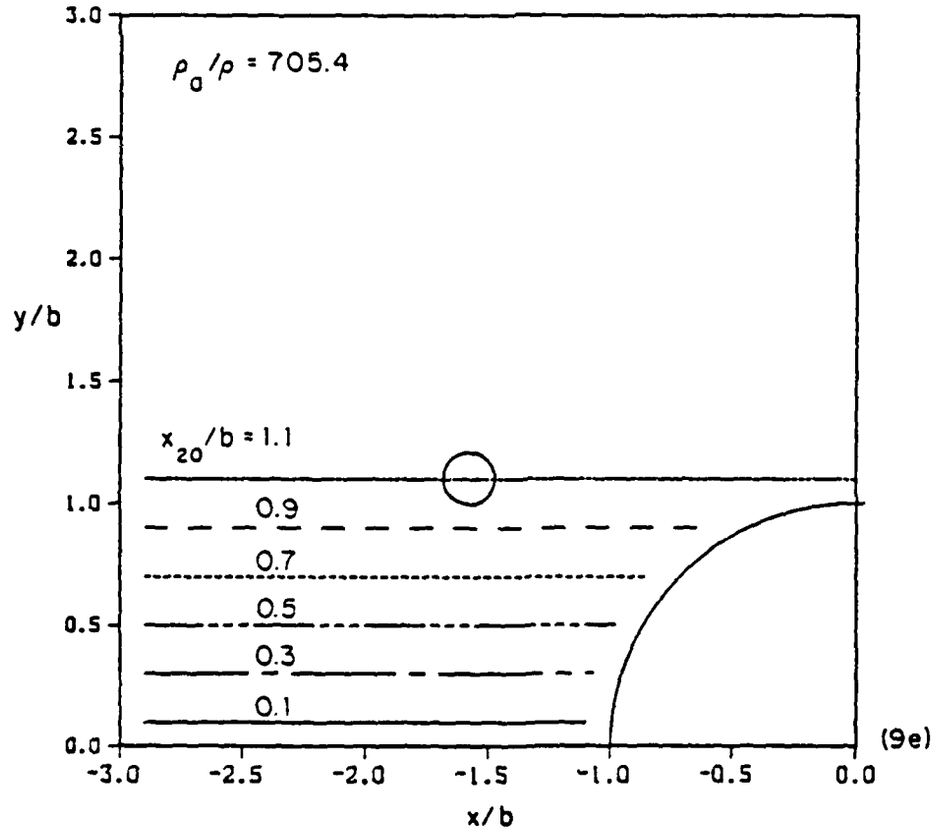


Figure 9. -- continued

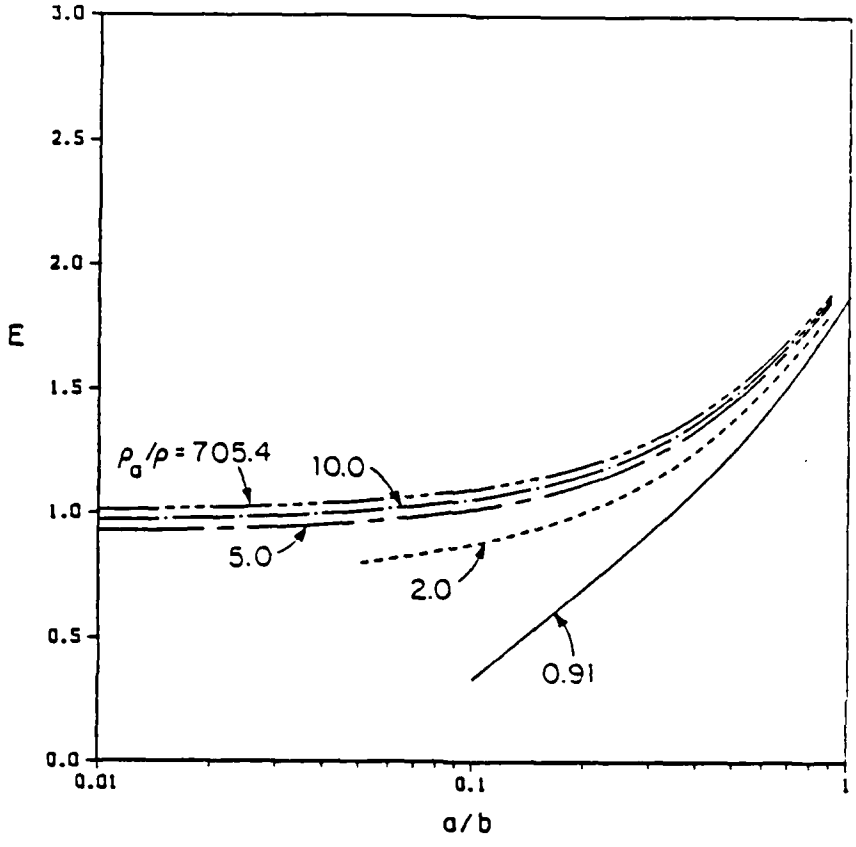


Figure 10. Dependence of the collection coefficient E of an ice particle on the size for various density ratios.

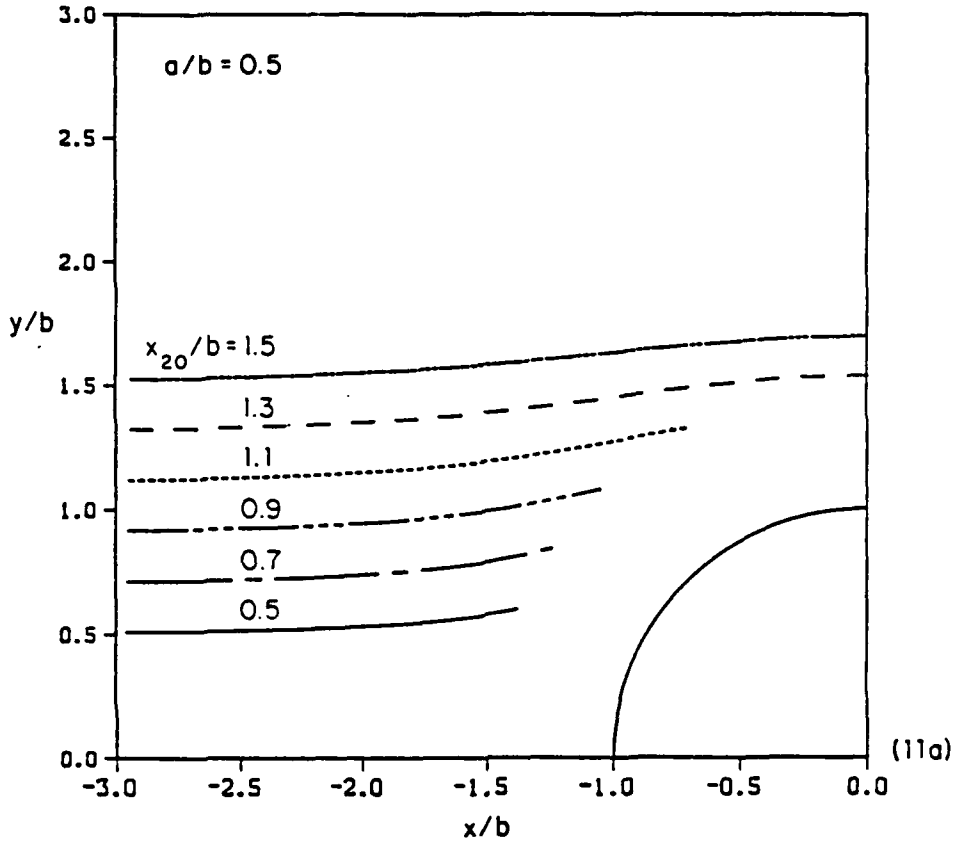


Figure 11. Trajectories of a moving sphere with $x_{1o}/b = -20$, $u_{1o}/U_o=1$, $u_{2o}/U_o= 0$, and $\rho_2/\rho = 0.89$.

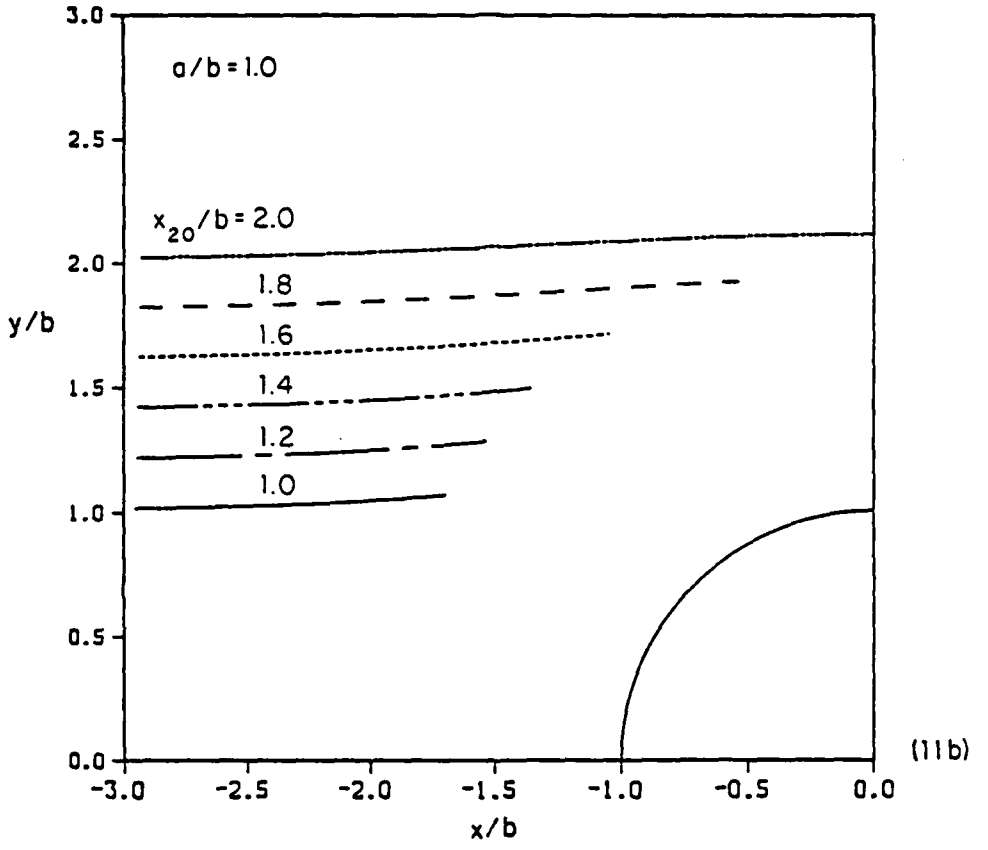


Figure 11. -- continued

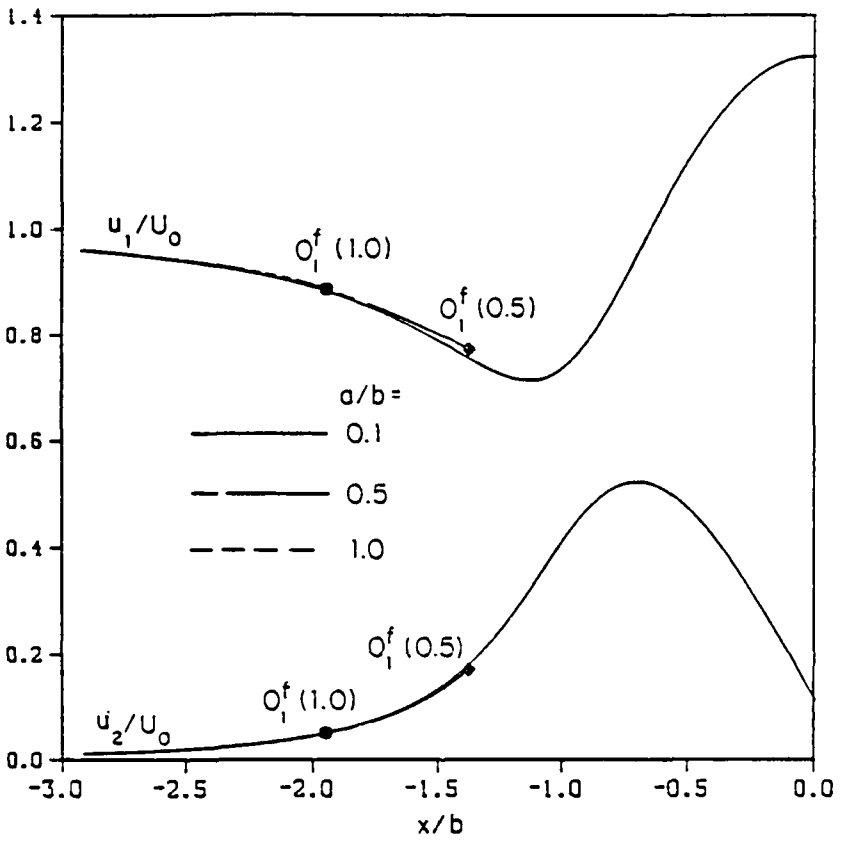


Figure 12. Velocity components $u_1$ and $u_2$ of a moving sphere with various radius ratios.

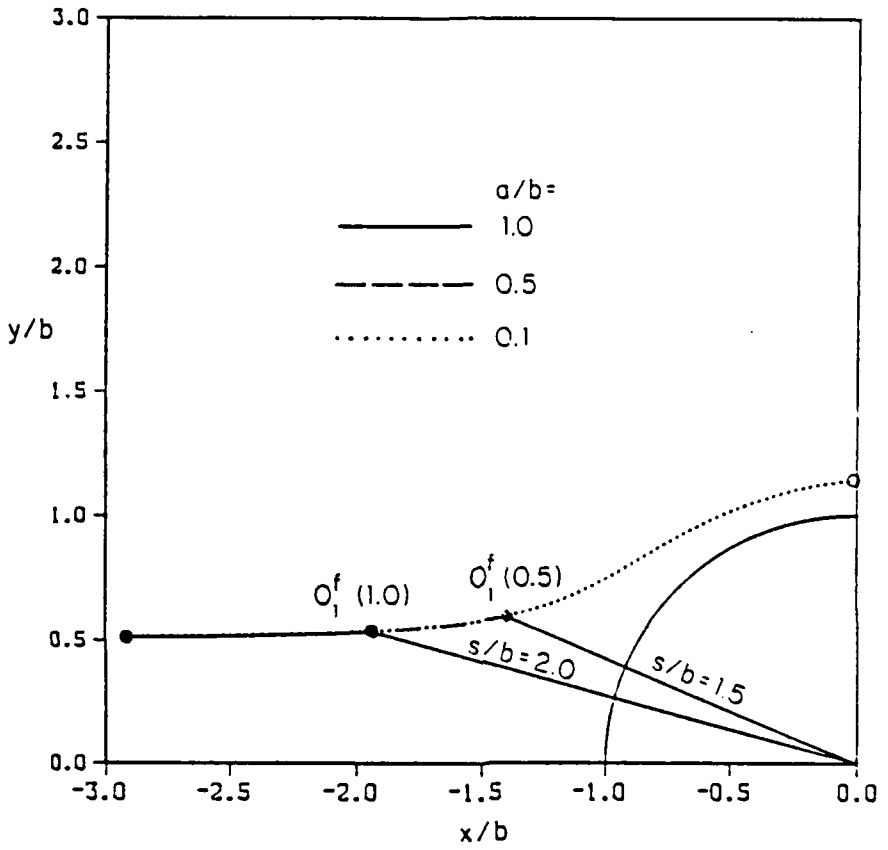


Figure 13. Trajectories of a moving sphere with various radius ratios.

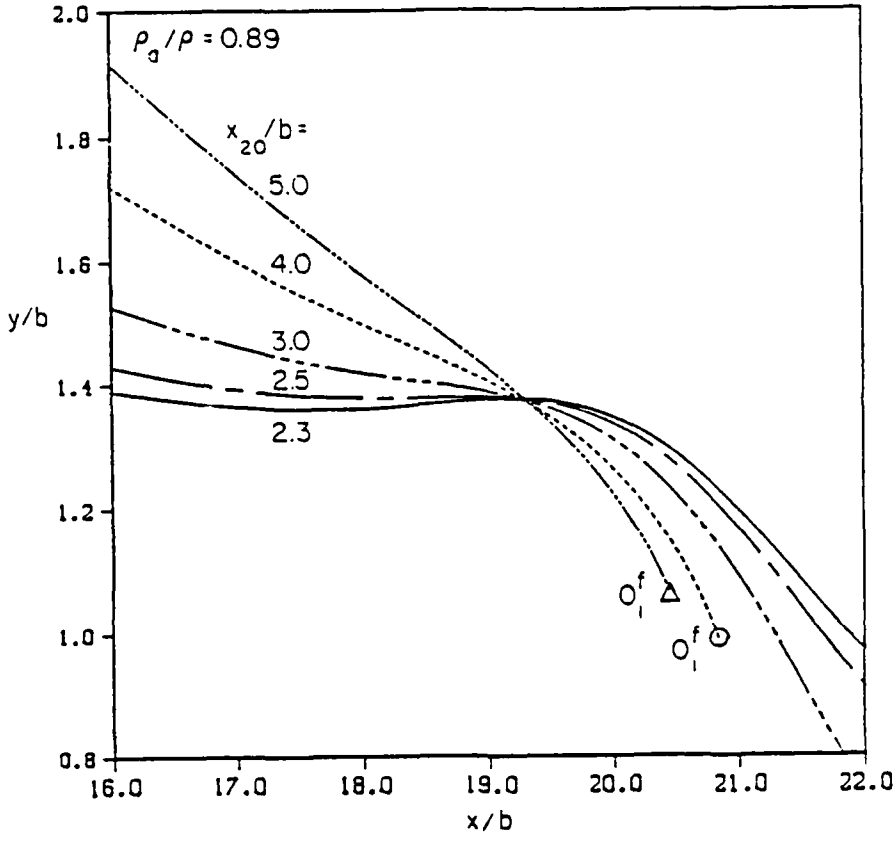


Figure 14. Trajectories of a moving sphere with radius a affected by another sphere with radius b, a/b=0.1, $\rho_a/\rho$ = 0.89.

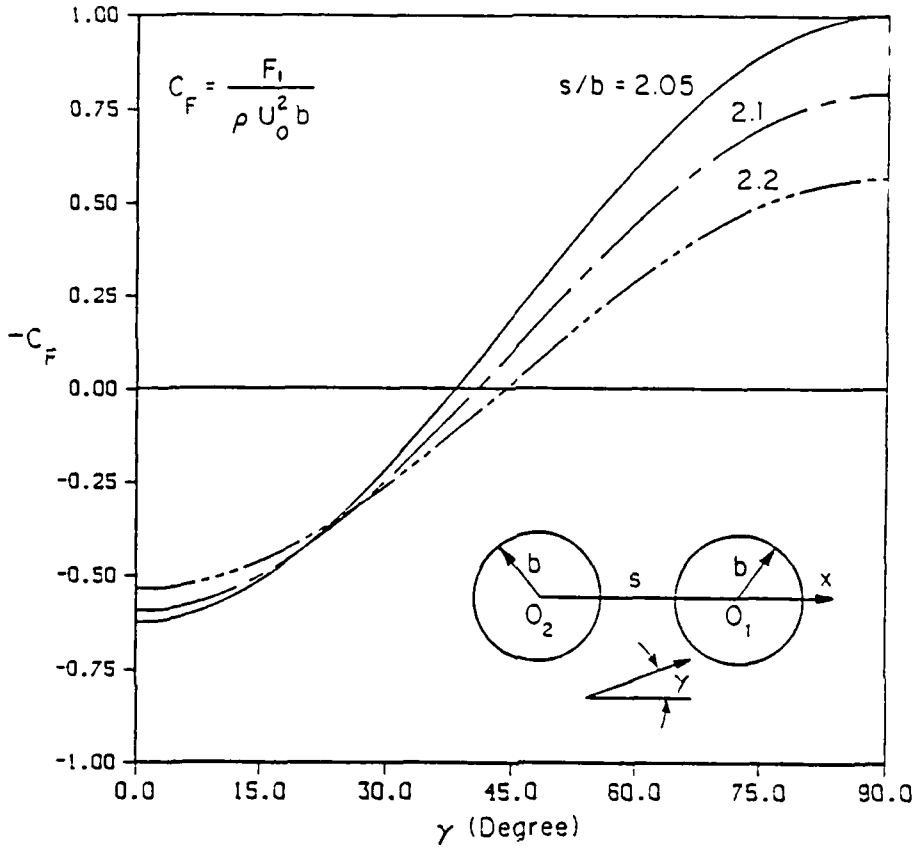


Figure 15. Dependence of interaction forces on the direction of a uniform flow.

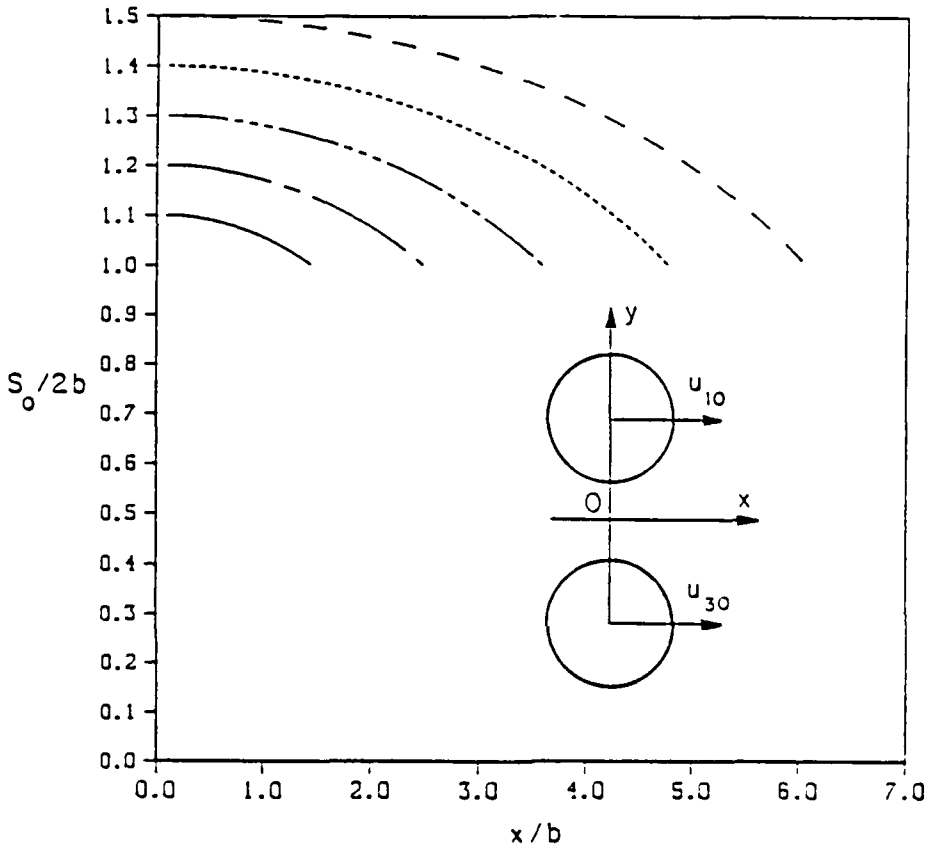


Figure 16. Trajectories of two equal spheres (a/b=1) moving initially perpendicular to their centerline in a stationary fluid with $\rho_s/\rho = 0.89$, a/b=1, $x_{1o}/b = x_{3o}/b = 0$, $u_{1o} = u_{3o} = 1$, and $u_{2o} = u_{4o} = 0$.

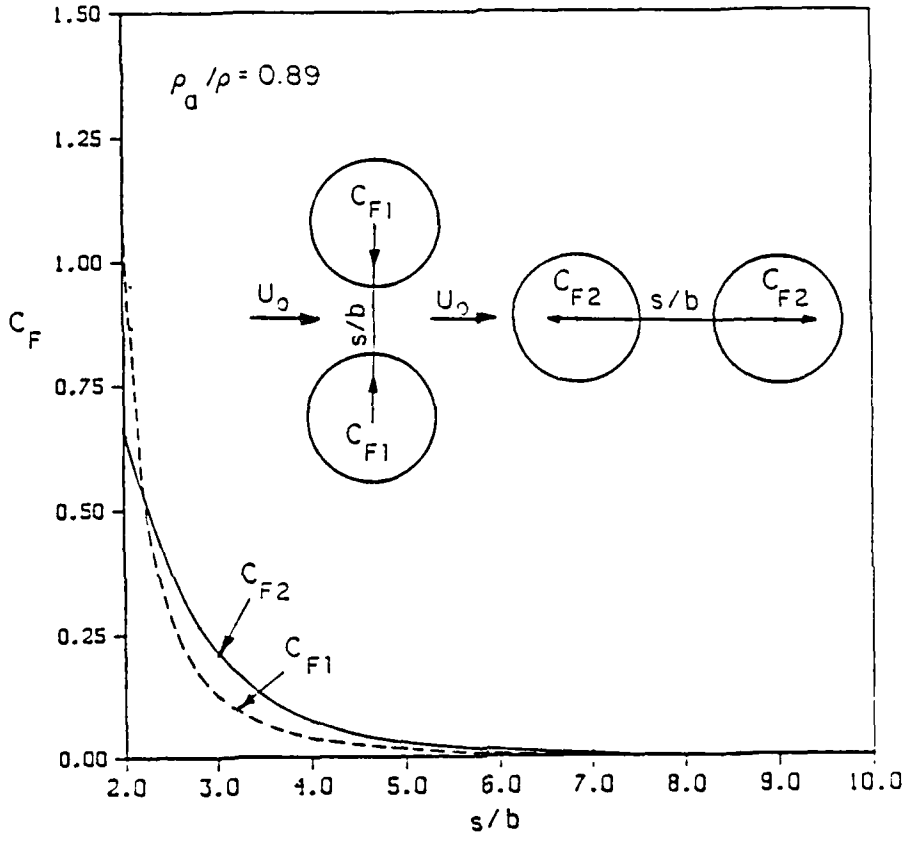


Figure 17. Interaction force between two equal spheres (a/b=1) versus the separation distance s/b.

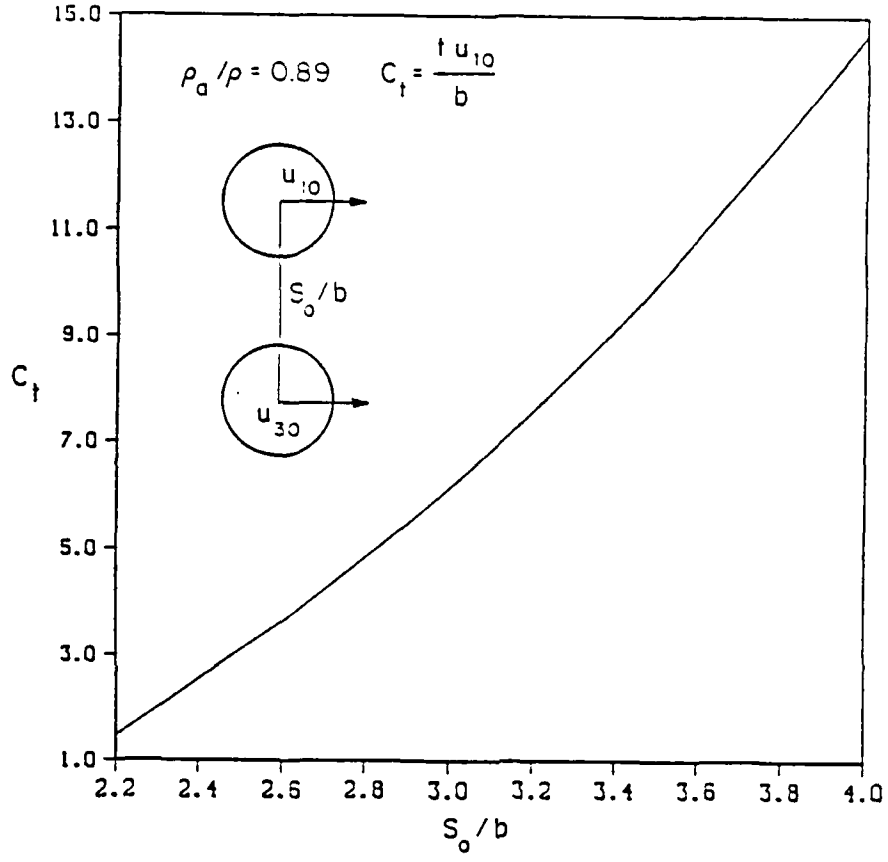


Figure 18. Time required for two equal spheres (a/b=1) to come into contact versus the separation distance $s_o/b$ with $\rho_a/\rho = 0.89$, $x_{1o}/b = x_{3o}/b = 0$, $u_{1o}=u_{3o}= 1$, and $u_{2o}=u_{4o}= 0$.

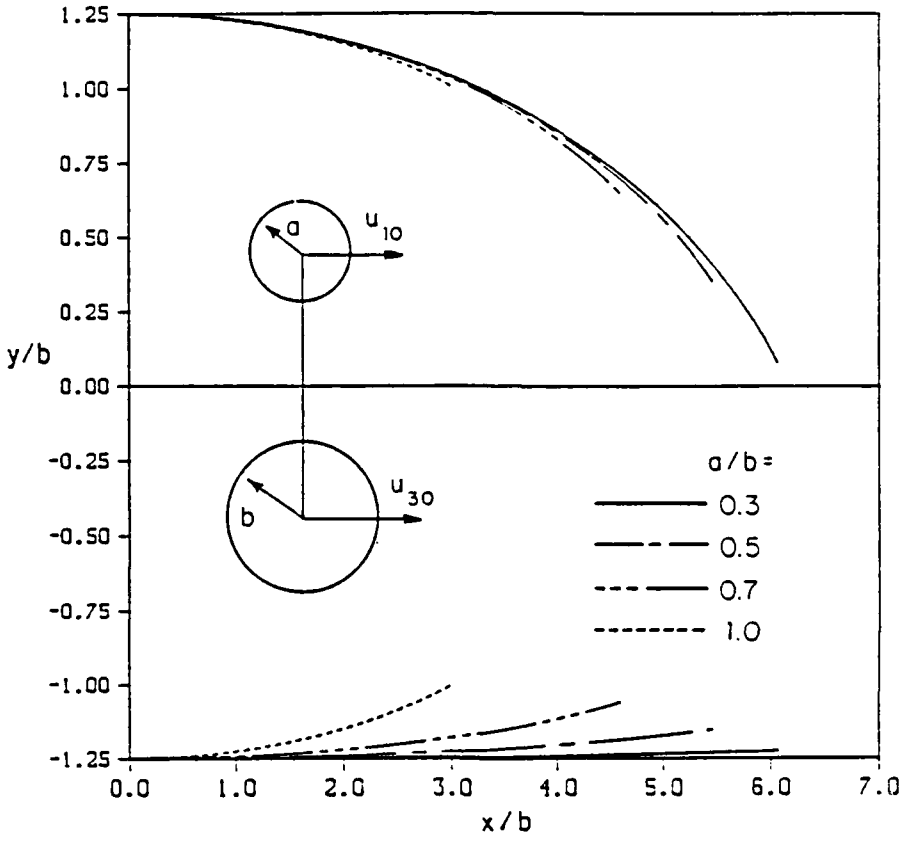


Figure 19. Trajectories of two spheres moving initially parallel to each other with $\rho_s/\rho = 0.39$, $x_{1o}/b = x_{3o}/b = 0$, $x_{2o}/b = -x_{4o}/b = 1.25$, $u_{1o}=u_{3o}= 1$, and $u_{2o}=u_{4o}= 0$.